Redox Biology 75 (2024) 103253

Contents lists available at ScienceDirect

Redox Biology

journal homepage: www.elsevier.com/locate/redox

Redox-modulated SNX25 as a novel regulator of GPCR-G protein signaling from endosomes

Yulong Zhang [a,b,1], Zhijun Yu [a,1], Mingwei Sun [c], Ruyue Du [a,b], Hanhan Gao [a,b], Qiankun Dai [a,b], Yan Dong [a,d,e], Cuicui Liu [f], Menghui Yin [a,b], Tingting Xu [a,d,e], Xiaofei Zhang [c,g], Jinsong Liu [a,b,d,e,**], Jinxin Xu [a,b,d,e,*]

[a] State Key Laboratory of Respiratory Disease, Guangzhou Institutes of Biomedicine and Health, Chinese Academy of Sciences, Guangzhou, 510530, China
[b] University of Chinese Academy of Sciences, Beijing, 100049, China
[c] Basic Research Center, Bioland Laboratory, Guangzhou Regenerative Medicine and Health Guangdong Laboratory, Guangzhou, 510530, China
[d] Guangdong Provincial Key Laboratory of Biocomputing, Guangzhou Institutes of Biomedicine and Health, Chinese Academy of Sciences, Guangzhou, 510530, China
[e] China-New Zealand Joint Laboratory on Biomedicine and Health, Guangzhou, 510530, China
[f] Guangzhou Institutes of Biomedicine and Health, Chinese Academy of Sciences, Guangzhou, 510530, China
[g] CAS Key Laboratory of Regenerative Biology, Guangdong Provincial Key Laboratory of Stem Cell and Regenerative Medicine, Center for Cell Lineage and Development, GIBH-HKU Guangdong-Hong Kong Stem Cell and Regenerative Medicine Research Centre, Guangzhou Institutes of Biomedicine and Health, Chinese Academy of Sciences, Guangzhou, Guangdong, 510530, China

ARTICLE INFO

Keywords:
GPCR
Endosomal signaling
G-protein
Sorting nexins (SNXs)
Regulator of G protein signaling (RGS)
Redox

ABSTRACT

GPCR-G protein signaling from endosomes plays a crucial role in various physiological and pathological processes. However, the mechanism by which endosomal G protein signaling is terminated remains largely unknown. In this study, we aimed to investigate the regulatory mechanisms involved in terminating the signaling of Gα subunits from endosomes. Through structural analysis and cell-based assays, we have discovered that SNX25, a protein that targets endosomes via its PXA or PXC domain, interacts with regulator of G protein signaling (RGS) proteins (including RGS2, RGS4, RGS8, and RGS17) in a redox-regulated manner. The interaction between SNX25 and these RGS proteins enhances their GTPase-accelerating activity towards $G\alpha_{i/q}$ and their ability to bind GDP-bound (inactive form) $G\alpha_{i/q}$. As a result, SNX25 recruits these RGS proteins to endosomes, leading to the termination of endosomal $G\alpha_{i/q}$ signaling. Furthermore, we have found that the SNX25/RGS complex also exerts a negative regulatory effect on $G\alpha_{i/q}$ signaling from the plasma membrane. This is achieved by recruiting $G\alpha_{i/q}$ to endosomes and preventing its activation on the plasma membrane. Our findings shed light on the previously unknown role of redox-modulated SNX25 in inhibiting $G\alpha_{i/q}$ signaling, thereby uncovering a novel mechanism for terminating $G\alpha_{i/q}$ signaling from endosomes. Importantly, this study expands our understanding of the regulation of GPCR-$G\alpha_{i/q}$ signaling beyond the plasma membrane.

1. Introduction

G protein-coupled receptors (GPCRs) are a class of signal transduction receptors that initiate various intracellular signaling reactions by promoting the switch of Gα subunits from their inactive GDP-bound form to the active GTP-bound form upon binding to different stimuli [1]. Upon activation, GPCRs on the cell surface undergo internalization and subsequently enter the endosomal pathway for degradation or recycling back to the plasma membrane [2,3]. Traditionally, it was believed that GPCRs become functionally activated only on the plasma membrane and are desensitized after internalization. However, accumulating evidence has demonstrated that certain internalized GPCRs retain their activity on endosomes, and their signaling from these compartments is necessary for gene transcription and oocyte meiosis [2,4,5]. Moreover, GPCR signaling from endosomes has been implicated in various physiological and pathophysiological processes, including skeletal homeostasis [6], hypercalcemia [7], diabetes [8], and irritable bowel syndrome [9]. While the molecular mechanisms underlying the desensitization of

* Corresponding author.
** Corresponding author.
E-mail addresses: liu_jinsong@gibh.ac.cn (J. Liu), xu_jinxin@gibh.ac.cn (J. Xu).
[1] These authors contributed equally.

https://doi.org/10.1016/j.redox.2024.103253
Received 24 May 2024; Accepted 20 June 2024
Available online 22 June 2024

endosomal GPCRs, such as the parathyroid hormone receptor (PTHR), have been investigated and involve intraluminal acidification and recycling trafficking [2,10,11], the mechanisms for terminating G protein signaling from endosomes remain largely unexplored.

The termination of G protein signaling involves the conversion of GTP-bound Gα subunits to GDP-bound Gα subunits through GTP hydrolysis, a process facilitated by the GTPase activity of Gα subunits [12]. Although the intrinsic GTPase activity of Gα subunits is relatively weak, this GTP hydrolysis can be significantly enhanced by binding to regulator of G protein signaling (RGS) proteins. RGS proteins from the R4, R7, and RZ subfamilies, which possess the canonical RGS domain, have been extensively studied as GTPase-activating proteins (GAPs) that promote the termination of G protein signaling on the plasma membrane [13].

Sorting nexins (SNXs) comprise a diverse group of proteins that are primarily involved in targeting the endosomal system through their Phox homology (PX) domain [14]. A subgroup of SNXs, known as SNX-RH (including SNX13, SNX14, and SNX25), has an N-terminal PXA domain, an RGS homology (RH) domain preceding the PX domain, and a C-terminal PXC domain [14,15]. This domain architecture suggests that SNX13, SNX14, and SNX25 may function as GTPase-activating proteins (GAPs) to enhance the termination of G protein signaling on endosomes. Among these SNX-RH proteins, SNX13 [16] and SNX14 [17] have been previously reported to play a role in regulating $G\alpha_s$-coupled GPCR signaling.

However, more recent investigations from our group have reported the crystal structures of the RH domain of SNX13 and SNX25, revealing that the non-canonical RH domains within the SNX-RH subgroup lack the ability to directly bind Gα subunits due to the absence of conserved residues [18]. Meanwhile, the significance of redox signaling in governing a wide range of fundamental biological processes, including gene expression and cell survival, has been extensively documented [19,20]. In this study, we employed mass spectrometry, structural analysis, and biochemical studies to identify several canonical RGS proteins, such as RGS2, RGS4, RGS8, and RGS17, that can interact with the PX domain of SNX25 under redox regulation. Through the recruitment of these canonical RGS proteins to endosomes, SNX25 facilitates the termination of endosomal $G\alpha_{i/q}$ signaling. Furthermore, the SNX25/RGS protein complex can modulate $G\alpha_{i/q}$ signaling originating from the plasma membrane by sequestering inactive $G\alpha_{i/q}$ subunits to endosomes. Collectively, our findings provide novel insights into the regulatory mechanism by which SNX25 governs $G\alpha_{i/q}$-coupled GPCR signaling from both endosomes and the plasma membrane.

2. Results

2.1. SNX25 interaction with RGS4 via the PX domain

In addition to the RGS homology (RH) domain, the PX domain of SNX25 has a unique feature - it lacks conserved residues necessary for PI3P binding [21]. To explore potential interaction partners for the RH domain and PX domain of SNX25, we conducted Flag immunoprecipitation followed by mass spectrometry (IP-MS) using HEK293T cells overexpressing a Flag-tagged RH-PX domain of mouse SNX25 (mSNX25) (Fig. 1A). Notably, our IP-MS assay revealed the presence of RGS4, a well-studied canonical RGS protein known to interact with Gα subunits in the $G\alpha_{i/o}$ and $G\alpha_{q/11}$ subfamilies (Fig. S1A). Moreover, reciprocal IP-MS experiments demonstrated that endogenous SNX25 can be precipitated by Flag-tagged RGS4, further supporting a potential interaction between the RH-PX domain of SNX25 and RGS4 (Fig. S1A).

To validate the interaction between the RH-PX domain of mSNX25 and RGS4, we performed a Co-immunoprecipitation (Co-IP) experiment. As expected, HA-tagged RGS4 co-purified with Flag-tagged RH-PX domain of mSNX25, confirming their interaction (Fig. 1B). Next, we aimed to identify the specific regions within the RH-PX domain that are essential for the binding of mSNX25 to RGS4. As shown in Fig. 1B, the $mSNX25^{RH-PX\Delta linker}$ variant, which lacks the linker region, maintained its ability to bind RGS4, while the $mSNX25^{RH\text{-}linker}$ variant did not. This suggests that the PX domain of SNX25 is crucial for its interaction with RGS4. Furthermore, we investigated whether the SNX25-PX domain alone is sufficient for binding to RGS4. Due to the low expression levels of the $mSNX25^{PX}$ domain in HEK293T cells, we generated a N-terminal extended PX domain construct called long-$mSNX25^{PX}$ (Fig. 1A). Notably, long-$mSNX25^{PX}$ retained the capacity to bind RGS4 (Fig. 1B).

To further investigate the interaction between SNX25 and RGS4 within cells, we conducted fluorescence co-localization analysis. RGS4 is a plasma membrane targeting protein mediated by its N-terminal region [22]. As demonstrated in Fig. 1C and Fig. S1B, $mSNX25^{PX}$-GFP was recruited to the plasma membrane by dsRed-RGS4, but not by the dsRed tag alone. This observation suggests that the PX domain of mSNX25 is involved in the recruitment of $mSNX25^{PX}$ to the plasma membrane via interaction with RGS4. We then examined whether the PX domain is essential for the full-length mSNX25 (mSNX25 FL) to associate with RGS4 in cells. In contrast to the mSNX25 PX domain alone, mSNX25 FL co-localized well with RGS4 in vesicle-like structures within cells (Fig. 1D). Conversely, RGS4 failed to be recruited significantly to the vesicle-like structures by mSNX25 lacking the PX domain (Fig. 1D). These findings collectively suggest that the PX domain is both necessary and sufficient for the association between SNX25 and RGS4.

2.2. Crystal structure of the PX domain of mSNX25

To gain insights into the molecular mechanism underlying the interaction between SNX25 and RGS4, we conducted structural studies on the PX domain of mSNX25 ($mSNX25^{PX}$). We successfully determined the crystal structure of mSNX25-PX domain at a resolution of 2.4 Å in space group $P6_122$, with five molecules in the asymmetry unit. The crystal structure of $mSNX25^{PX}$ revealed a conventional PX domain fold, consisting of three β strands followed by three α helices. However, unlike the canonical highly positive charged phosphoinositide (PI) binding pocket, the postulated PI binding pocket in $mSNX25^{PX}$ is distinct, which is filled with hydrophobic residues M527, L553, and L578, as well as negatively charged residues E522 and E525 (Fig. 2A). This structural observation is consistent with previous findings [21] that the PX domain of SNX25 lacks the canonical capacity to bind phosphoinositides.

In addition, we observed the presence of a homodimer of $mSNX25^{PX}$ in the crystal structure. Remarkably, the dimeric interface is stabilized by an inter-chain disulfide bond formed by residue C566, which is located on the tail of α1 from two $mSNX25^{PX}$ molecules (Fig. 2B). Sequence alignment analysis revealed that this cysteine residue is highly conserved from humans to frogs. Interestingly, a previous study from our group reported the existence of a thiol-modulated homodimer of the zebrafish SNX25 PX domain [23]. That dimerization was also mediated by the conserved cysteine residue, as confirmed by gel filtration and mass spectrometry data. These findings suggest that the conserved cysteine residue on the tail of α1 within the PX domain can undergo oxidation, potentially playing a functional role in the evolutionary adaptation of SNX25.

2.3. SNX25 association with canonical RGS proteins may be regulated by redox reaction

To investigate the importance of the conserved C566 residue in the interaction between SNX25 and RGS4, we performed Co-IP experiments using mutated mSNX25. The results of the Co-IP experiment showed that the ability of $mSNX25^{RH-PX}$ binding to RGS4 was nearly abolished when C566 was mutated to alanine (C566A) (Fig. 3A). Moreover, the $mSNX25^{PX}$ C566A mutant displayed a diffuse distribution throughout the entire cell, and failed to be recruited to the plasma membrane by RGS4 (Fig. 3B and Fig. S1B). Additionally, the mSNX25C566A mutant was unable to recruit RGS4 to vesicles (Fig. 3C). These findings indicate that C566 is crucial for the interaction between mSNX25 and RGS4.

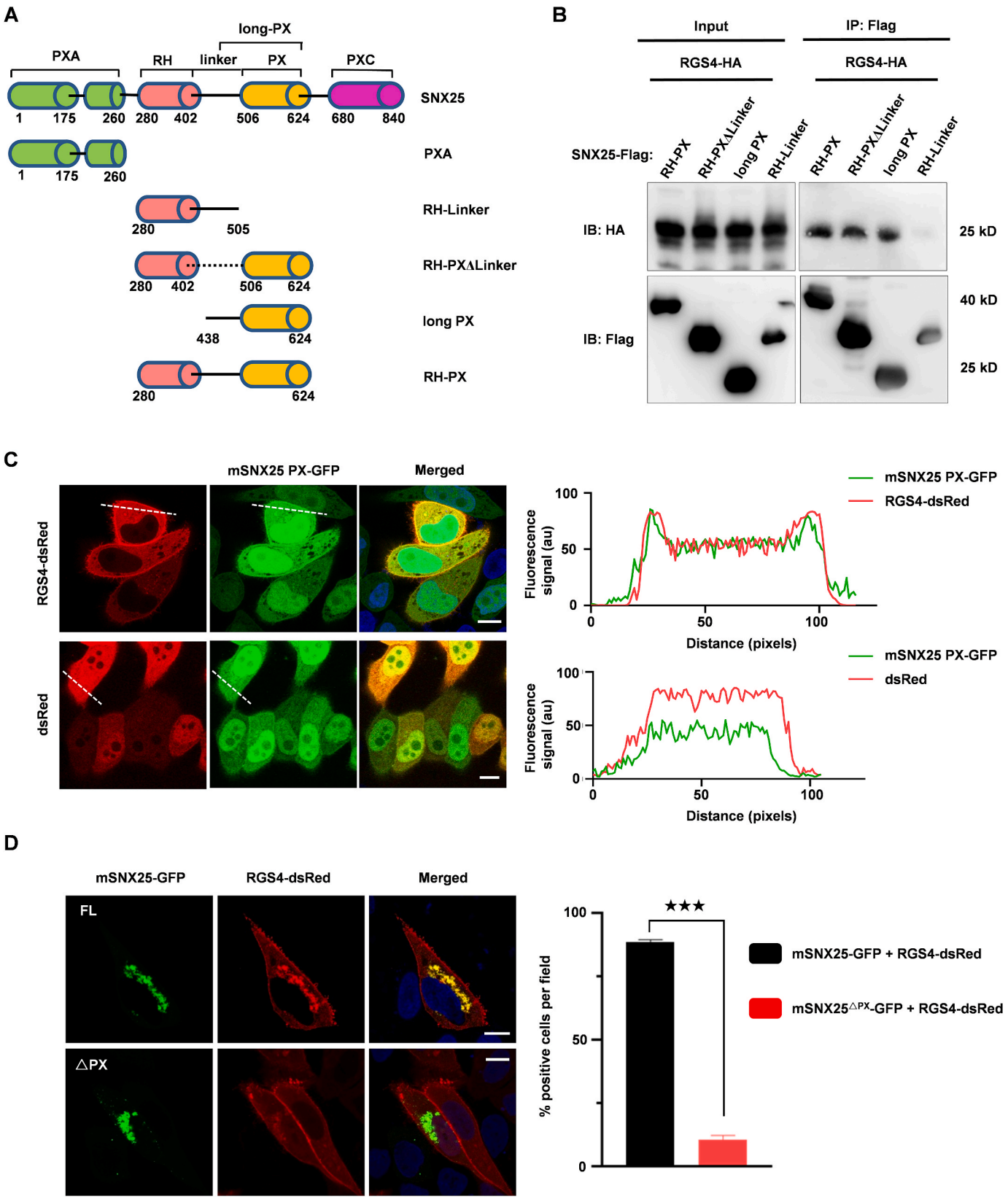

Fig. 1. PX domain of SNX25 interaction with RGS4. (A) Domain architecture of mSNX25. PX, phox-homology; PXA, PX-associated domain A; RH: RGS homology domain; PXC, PX-associated domain C. (B) Co-immunoprecipitation indicates that PX domain is essential for mSNX25 association with RGS4. Flag-tagged fragment of mSNX25 was co-transfected with HA-RGS4 into HEK293T cells. Co-IP was performed with anti-Flag magnetic beads, after 48 h of transfection. (C) mSNX25-PX domain co-localization with RGS4 on the plasma membrane. GFP and dsRed linear profiles were made by RGB Profiler (ImageJ), which span the entire cell. (D) Subcellular distribution of mSNX25 and RGS4 in HeLa cells. Quantification of colocalization cells for mSNX25 (WT or ΔPX) and RGS4 were taken from lower-magnification wide-field images. Data represents the average from n = 5 experiments, error bars represent SEM, 5 visual fields and 100^{+} cells per condition. ★★★P < 0.001 by unpaired student's *t*-test. Scale bars, 10 μm.

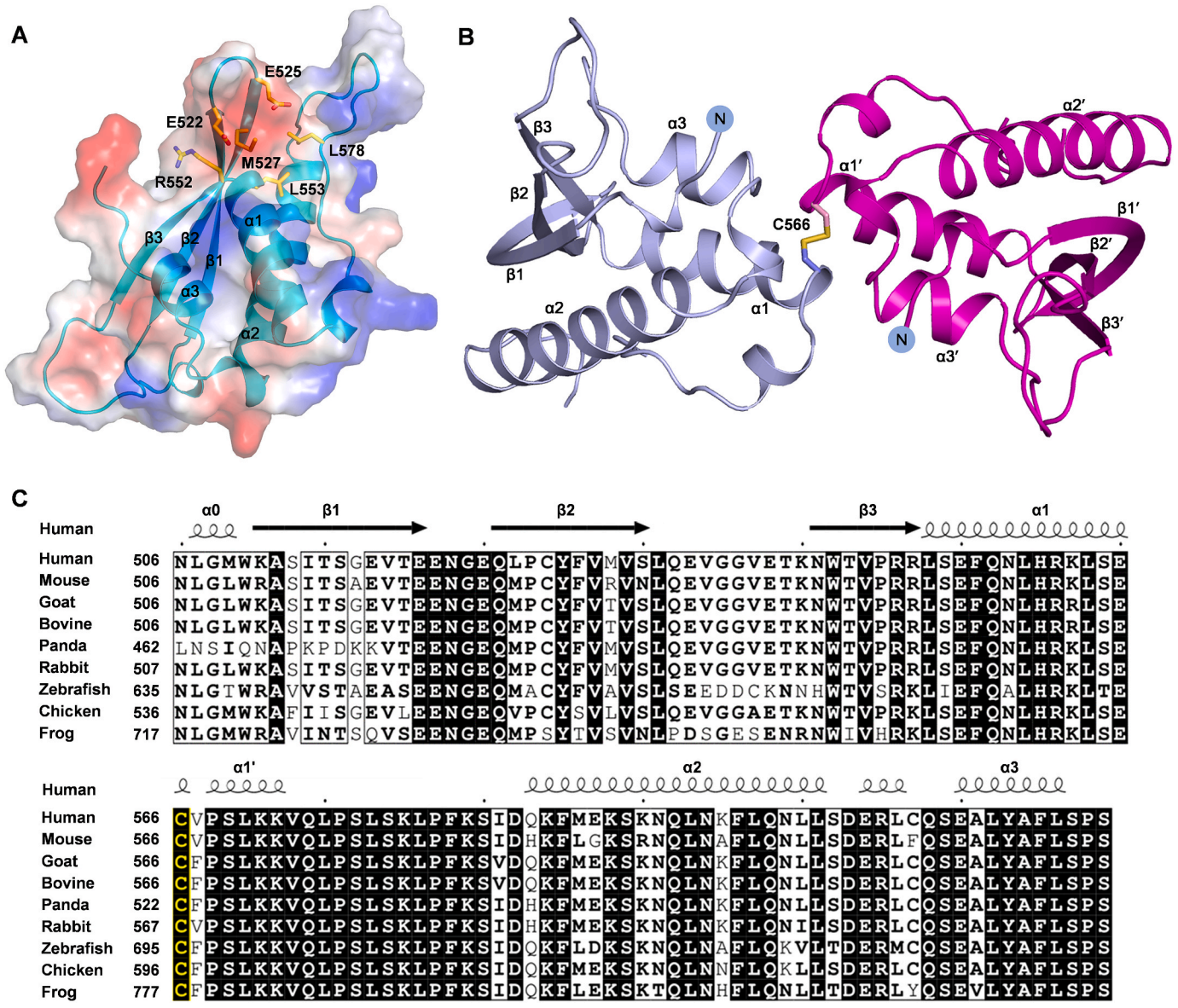

Fig. 2. Overall structure of mSNX25^{PX}. (A) Structure of mSNX25^{PX} was shown as cyan cartoon and surface potential. (B) Thiol modulated homo-dimer of mSNX25^{PX}. Two molecules were colored as magenta and light blue cartoon, respectively. (C) Sequence alignment of SNX25^{PX} from different species. The conserved C566 was highlight in yellow. (For interpretation of the references to color in this figure legend, the reader is referred to the Web version of this article.)

To investigate whether RGS4 interacts with the monomeric form or the thiol-modulated dimer form of mSNX25^{PX}, we purified the monomeric mSNX25^{PX} with a C-terminal 6 × His tag that was expressed in bacteria. To obtain the thiol-modulated dimer of mSNX25^{PX}, the monomer was treated with H_2O_2 and then purified using gel filtration. The purified mSNX25^{PX} monomer and the dimer formed by H_2O_2 oxidation were subjected to a co-immunoprecipitation assay with Flag-RGS4 from HEK293T cell extracts. As depicted in Fig. 3D, only the mSNX25^{PX} monomer was immunoprecipitated with Flag-RGS4. Interestingly, the mSNX25^{PX} dimer produced by H_2O_2 oxidation could be transformed into monomer (m^{D}) after treatment with DTT, indicating that the dimer is dependent on the disulfide bond. Importantly, the mSNX25^{PX} monomer (m^{D}) retained its binding capacity to RGS4 (Fig. 3D). These results suggest that RGS4 interacts specifically with the monomeric form of mSNX25^{PX} but not the thiol-modulated dimer of mSNX25^{PX}.

Based on above results, we hypothesized that C566 on mSNX25^{PX} could form a disulfide bond with a cysteine residue on RGS4. To investigate this, we conducted co-IP experiments in the presence or absence of DTT. As expected, the interaction between mSNX25^{RH-PX} and RGS4 was completely disrupted by the addition of 5 mM DTT (Fig. 3E). Further analysis revealed that both the flexible N-terminal domain and the C-terminal RGS domain of RGS4 contain multiple cysteine residues (Figs. S2A–B). To determine which cysteine residue on RGS4 is essential for its interaction with SNX25, we generated truncation mutants of RGS4. The results demonstrated that the N-terminal domain of RGS4 is indispensable for binding to mSNX25^{RH-PX}, as deletion of this domain abolished the interaction (Fig. 3E). Additionally, when all four cysteine residues on the N-terminal domain were mutated to alanine (NC-A), the RGS4 mutant failed to interact with mSNX25 (Fig. 3F). Interestingly, mutating any single cysteine residue on the N-terminal domain did not significantly affect RGS4 binding to mSNX25, suggesting that these cysteine residues may act collectively in mediating the interaction. To test which of the four cysteine residues on the N-terminal domain involve in RGS4 interaction with mSNX25, and to exclude the possibility that these cysteine residues contribute to this interaction by forming intramolecular disulfide bridge, we constructed four mutants of RGS4 that retain only one of the four cysteine residues

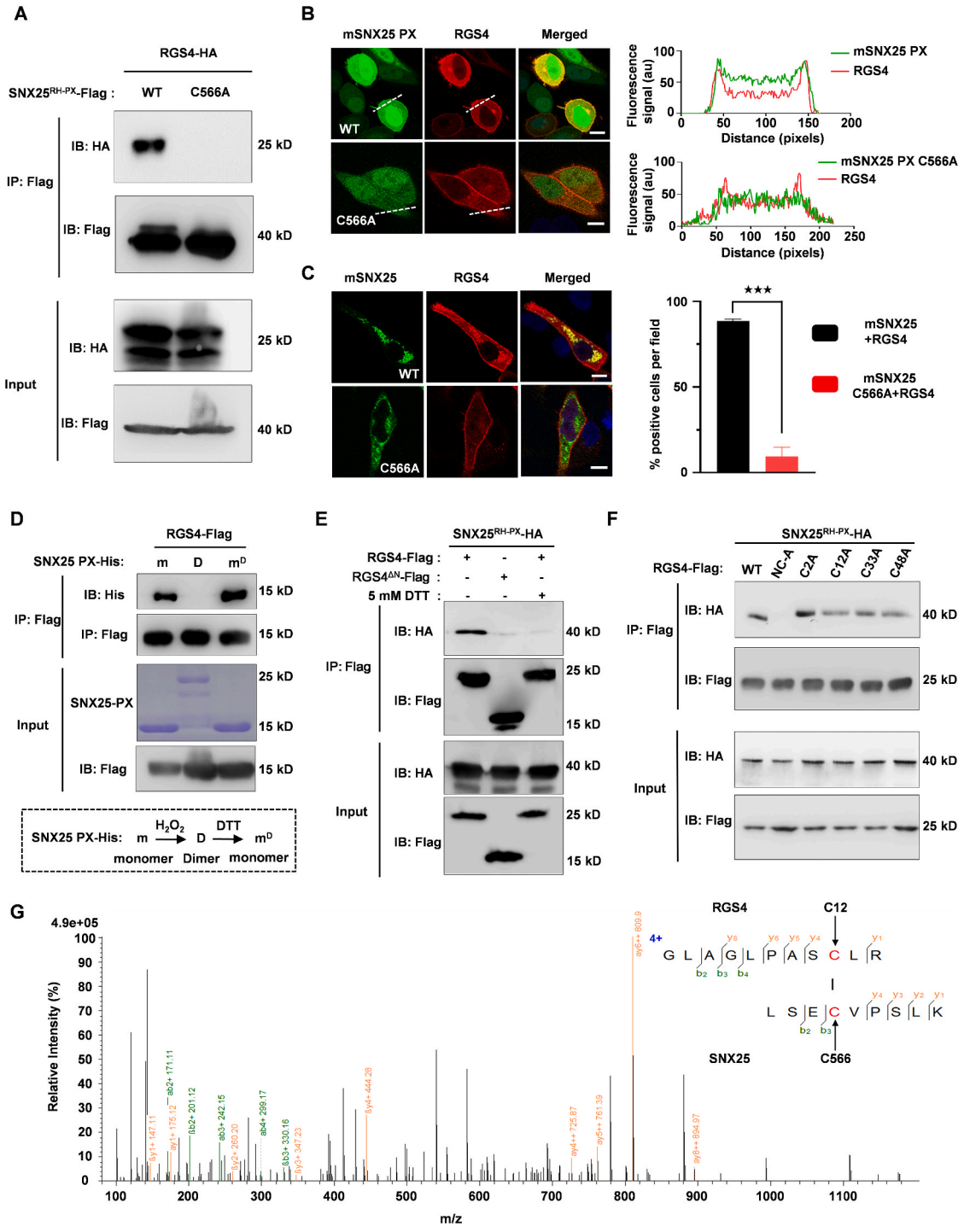

Fig. 3. SNX25 interacts with RGS4 mediated by disulfide bond. (A) Co-immunoprecipitation indicates the importance of C566 for mSNX25^{RH-PX} association with RGS4. Flag tagged mSNX25^{RH-PX} (wild type or C566A mutant) and HA tagged RGS4 were co-transfected into HEK293T cells. Co-IP was performed with anti-Flag beads, after 48 h of transfection. (B) Subcellular distribution of dsRed tagged RGS4 and GFP tagged mSNX25-PX domain (wild type or C566A mutant) in HeLa cells. GFP and dsRed linear profiles were made by RGB Profiler (ImageJ), which span the entire cell. (C) Subcellular distribution of dsRed tagged RGS4 and GFP tagged full length of mSNX25 (wild type or C566A mutant) in HeLa cells. Quantification of colocalization cells for mSNX25 and RGS4 were taken from lower-magnification wide-field images. Data represents the average from n = 5 experiments, error bars represent SEM, 5 visual fields and 100+ cells per condition. ***$P < 0.001$ by unpaired student's *t*-test. (D) Co-immunoprecipitation analysis RGS4 interaction with monomer or dimer form of mSNX25^{PX}. mSNX25^{PX} and RGS4-Flag were expressed in bacteria and HEK293T, respectively. Purified mSNX25^{PX} was mixed with lysate of HEK293T expressing RGS4 prior to co-immunoprecipitation with anti-Flag beads. m: untreated monomer of mSNX25^{PX}; D: SNX25^{PX} dimer produced by oxidizing the monomer with H_2O_2; m^D: mSNX25^{PX} monomer that produced by reducing H_2O_2 induced dimer form mSNX25^{PX}. For the input of mSNX25^{PX}, the SDS-PAGE was performed without reducing agent. For other samples, the SDS-PAGE was performed with 0.7 M β-mercaptoethanol. (E) Co-immunoprecipitation indicates the importance of N-terminal domain for RGS4 association with mSNX25^{RH-PX}. (F) Co-immunoprecipitation indicates the importance of cysteine residues on N-terminal domain for RGS4 association with mSNX25^{RH-PX}. NC-A: cysteine residues on N-terminal domain of RGS4 were mutated to Ala. (G) MS identification disulfide bond between RGS4 and mSNX25. For (B–C), Scale bars, 10 μm.

on the N terminal domain, with all the other 10 cysteine residues on RGS4 mutated. Here, we named the four mutants as RGS4$^{m10\text{-}C2}$ (retaining C2), RGS4$^{m10\text{-}C12}$ (retaining C12), RGS4$^{m10\text{-}C33}$ (retaining C33) and RGS4$^{m10\text{-}C48}$ (retaining C48), respectively. Co-IP assay showed that RGS4$^{m10\text{-}C2}$, RGS4$^{m10\text{-}C12}$ and RGS4$^{m10\text{-}C33}$, but not RGS4$^{m10\text{-}C48}$, could effectively interact with mSNX25 (Fig. S3). As a negative control, RGS4^{m11} (all cysteine residues were mutated) lost the ability binding to mSNX25 (Fig. S3).

To further confirm the formation of a disulfide bond between the cysteine residue on the N-terminal domain of RGS4 and C566 of mSNX25, we performed mass spectrometry analysis on the purified RGS4/mSNX25^{RH-PX} complex obtained through co-immunoprecipitation from HEK293T cell lysate. The mass spectrometry results revealed the presence of an inter-chain disulfide bond between C566 of mSNX25 and C12 of RGS4 (Fig. 3G), while the disulfide bond cannot be observed for the other three cysteine residues on the N terminal domain of RGS4. This may imply that C12 is the primary residue for RGS4 forming disulfide bond with C566 of mSNX25. This result is consistent with our Co-IP experiment that RGS4$^{m10\text{-}C12}$ is more potent than other three mutants (RGS4$^{m10\text{-}C2}$, RGS4$^{m10\text{-}C133}$ and RGS4$^{m10\text{-}C48}$) in binding to mSNX25. Taken together, these findings provide strong evidence that SNX25 interacts with RGS4 via an intermolecular disulfide bond.

In addition to RGS4, we also investigated the interaction of SNX25 with other members of the R4 and RZ subfamilies, including RGS2, RGS8, and RGS17 (Figs. S2A–B). Similar to RGS4, we found that RGS2, RGS8, and RGS17 could be co-immunoprecipitated with mSNX25^{RH-PX} (Fig. S4) and co-localized with mSNX25 in cells (Figs. S5A and B). Further analysis revealed that these interactions were dependent on both C566 in mSNX25 (Figs. S5A–F) and a cysteine residue in the N-terminal domain of the respective RGS proteins (Fig. S4). Mass spectrometry analysis successfully detected the presence of an inter-chain disulfide bond between C566 of mSNX25 and either C19 or C27 of RGS8 (Fig. S6). Collectively, these results demonstrate that the interaction between SNX25 and RGS proteins is primarily stabilized by a disulfide bond between C566 in mSNX25 and a cysteine residue in the N-terminal domain of RGS proteins. This suggests that the association of SNX25 with RGS proteins may be regulated by redox processes.

2.4. SNX25 recruits both active and inactive form $G\alpha_{i/q}$ subunits to endosomes by cooperation with RGS proteins

Our recent research has revealed that the RGS homology domain (RH domain) of SNX25 is unable to directly interact with Gα subunits [18]. However, since canonical RGS proteins can interact with active form Gα subunits, we hypothesized that SNX25 might associate with Gα subunits indirectly through its interaction with canonical RGS proteins. Indeed, our experiments demonstrated that in the presence of RGS4, the over-expressed $G\alpha_i$ could be immunoprecipitated by mSNX25^{RH-PX} (Fig. 4A). Interestingly, even in the absence of aluminum magnesium fluoride (AMF), which is used to stabilize the active form of Gα subunits, $G\alpha_i$ was still able to associate with the mSNX25^{RH-PX}/RGS4 complex (Fig. 4A). Importantly, this interaction was dependent on C566 in the PX domain of mSNX25 (Fig. S7A). Then, we ask whether this interaction can be detected for endogenous proteins. To test this, co-immunoprecipitation assays were applied with neuroblast cell line IMR-32. As expected, endogenous RGS4 and $G\alpha_i$ could be co-immunoprecipitated by endogenous SNX25, in the presence or absence of AMF (Figs. S7B–C). Also, this interaction is impaired by the addition of 5 mM DTT. These Co-IP experiments suggest that the mSNX25/RGS4 complex can interact with $G\alpha_i$ subunits in both their active and inactive forms.

Furthermore, our analysis of cellular distribution revealed that mSNX25, in cooperation with RGS4, could recruit $G\alpha_i$ to vesicular structures (Fig. 4B and Fig. S7D). To further confirm that the mSNX25^{RH-PX}/RGS4 complex can bind to both active and inactive forms of $G\alpha_i$ subunits in cells, we conducted subcellular distribution analysis using constitutively active (Q204L) [24] and inactive (G42R) [25] mutant forms of $G\alpha_i$ subunits. Our results demonstrated robust co-localization of both the $G\alpha_i$ Q204L mutant and the G42R mutant with mSNX25 and RGS4 on vesicular structures (Fig. 4C and Fig. S7E).

Additionally, when mSNX25 cooperated with RGS8 or RGS17, there was a significant enhancement in its binding capacity to $G\alpha_i$ (Figure S7A, S8A-B). In addition to its interaction with $G\alpha_i$ subunit, it has been reported that both RGS4 and RGS8 can also interact with the $G\alpha_q$ subunit. Consistent with this, our experiments showed that $G\alpha_q$, but not $G\alpha_s$, could be recruited by the mSNX25/RGS4 complex in cells (Fig. 4B and Fig. S7D). Furthermore, the co-immunoprecipitation experiment demonstrated that $G\alpha_q$ bound to the mSNX25^{RH-PX}/RGS8 complex independently of aluminum magnesium fluoride (AMF) (Fig. 4D). Co-localization analysis also revealed that both the constitutively active (Q209L) [24] and inactive (G48R) [25] mutant forms of the $G\alpha_q$ subunit co-localized with mSNX25 and RGS8 on vesicular structures (Fig. 4E and Fig. S8C).

The recruitment of RGS proteins and Gα subunits to vesicular structures led us to speculate that SNX25 might localize to endosomes. To confirm this, we examined the co-localization of mSNX25 with the well-known endosome marker FYVE. Our results demonstrated significant co-localization of mSNX25 with FYVE, providing evidence for the endosomal distribution of mSNX25 (Fig. 4F and Fig. S9A). Furthermore, mSNX25 co-localized with RGS2, RGS4, RGS8, or RGS17 on endosomes (Fig. 4G and Fig. S9B). The structural analysis of mSNX25 identified an unconventional phosphoinositide (PI) binding pocket in its PX domain, which cannot associate with the endosome-characteristic phosphoinositide PI3P. Therefore, we investigated which domain of mSNX25 is responsible for mediating its association with endosomes. Co-localization assays revealed that the RH-PX domain of mSNX25 lost the ability to co-localize with FYVE (Figs. S9A and C). In contrast, the PXA domain and PXC domain showed notable co-localization with FYVE, suggesting that mSNX25's targeting to endosomes is mediated by its PXA domain or PXC domain (Fig. 4F and Fig. S9A). Taken together, our results demonstrate that both the active and inactive forms of $G\alpha_i$ and $G\alpha_q$ subunits can be recruited to endosomes by SNX25 in cooperation with canonical RGS proteins.

2.5. SNX25 promotes the GAP activity of targeted canonical RGS proteins

The interaction between SNX25 and canonical RGS proteins raises the question of whether the GTPase activating protein (GAP) activity of canonical RGS proteins is retained in the presence of SNX25. Initially, we attempted to obtain the complex of mSNX25^{RH-PX} and RGS protein (RGS4, RGS8, or RGS17) by simply mixing purified mSNX25^{RH-PX} and RGS protein. However, we failed to obtain this complex (data not shown). Nonetheless, we were able to successfully purify the complex of mSNX25^{RH-PX} with canonical RGS proteins (RGS4, RGS8, or RGS17) using anti-Flag affinity chromatography in HEK293F cells co-expressing Flag-tagged mSNX25^{RH-PX} and HA-tagged RGS proteins. To assess the impact of the mSNX25^{RH-PX}/RGS protein complex on GTP hydrolysis activity, we performed GTPase assays. Our results demonstrated that the presence of the mSNX25^{RH-PX}/RGS4, mSNX25^{RH-PX}/RGS8, or mSNX25^{RH-PX}/RGS17 complex significantly accelerated the GTP hydrolysis activity of the $G\alpha_i$ subunit (Fig. 5A). Similarly, the GTP hydrolysis activity of the $G\alpha_q$ subunit was enhanced in the presence of the mSNX25^{RH-PX}/RGS2, mSNX25^{RH-PX}/RGS4, mSNX25^{RH-PX}/RGS8, or mSNX25^{RH-PX}/RGS17 complex (Fig. 5B).

Previous studies have reported that residues N128 and D163 in RGS4 are essential for its GAP activity [26], and Y84 is critical for RGS4 binding to the $G\alpha_i$ or $G\alpha_q$ subunit [18]. To confirm the importance of these residues, we mutated N128/D163 to Ala and Y84 to Gly in RGS4. Our results showed that the GAP activity was abolished in both the mSNX25^{RH-PX}/mutated RGS4 complex and the mutated RGS4 (Fig. 5C and Fig. S10A). These findings suggest that the GAP activity of the

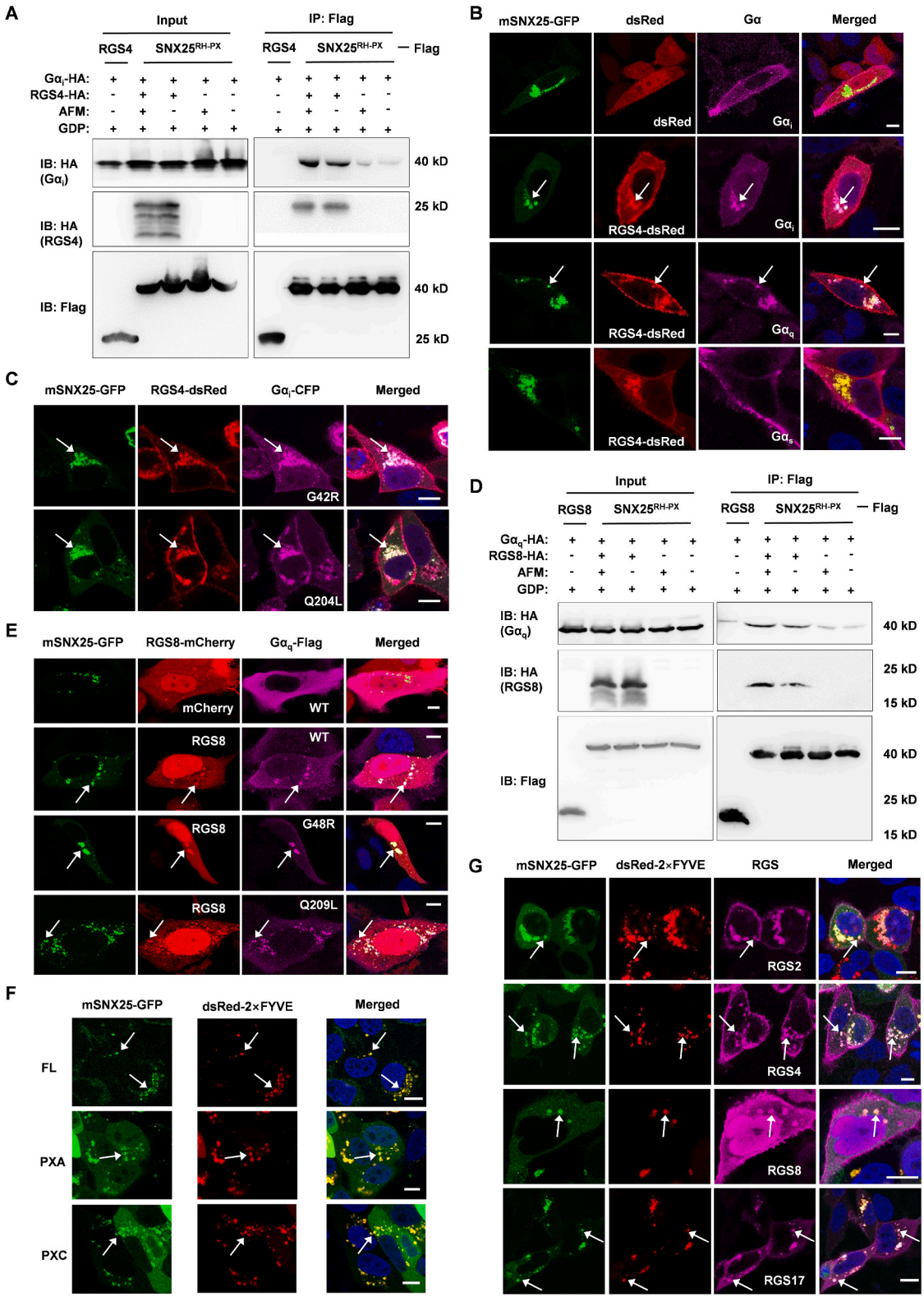

Fig. 4. SNX25 recruits $G\alpha_i$ or $G\alpha_q$ subunit to endosomes through interaction with canonical RGS proteins. (A) Co-immunoprecipitation indicates that mSNX25^{RH-PX} interactions with active or inactive form $G\alpha_i$ in the presence of RGS4. AMF, aluminum magnesium fluoride. (B) Subcellular localization of mSNX25 together with RGS4, and Gα subunit ($G\alpha_i$, $G\alpha_q$ or $G\alpha_s$) in HeLa cells. The $G\alpha_i$ subunit was tagged with CFP at the C-terminus. The $G\alpha_q$ and $G\alpha_s$ subunits were tagged with Flag at the C-terminus. (C) Subcellular localization of mSNX25 together with RGS4, and constitutively active (Q204L) or inactive (G42R) $G\alpha_i$ subunit in HeLa cells. (D) Co-immunoprecipitation indicates that mSNX25^{RH-PX} interacts with active or inactive form $G\alpha_q$ in the presence of RGS8. AMF, aluminum magnesium fluoride. (E) Subcellular localization of mSNX25 together with RGS8, and wild type, constitutively active (Q209L) or inactive (G48R) $G\alpha_q$ subunit in HeLa cells. (F) Subcellular localization of mSNX25, PXA domain or PXC domain together with early endosome marker FYVE in HeLa cells. (G) Subcellular localization of mSNX25 together with canonical RGS protein (RGS2, RGS4, RGS8 or RGS17), and early endosome marker FYVE in HeLa cells. Scale bars, 10 μm.

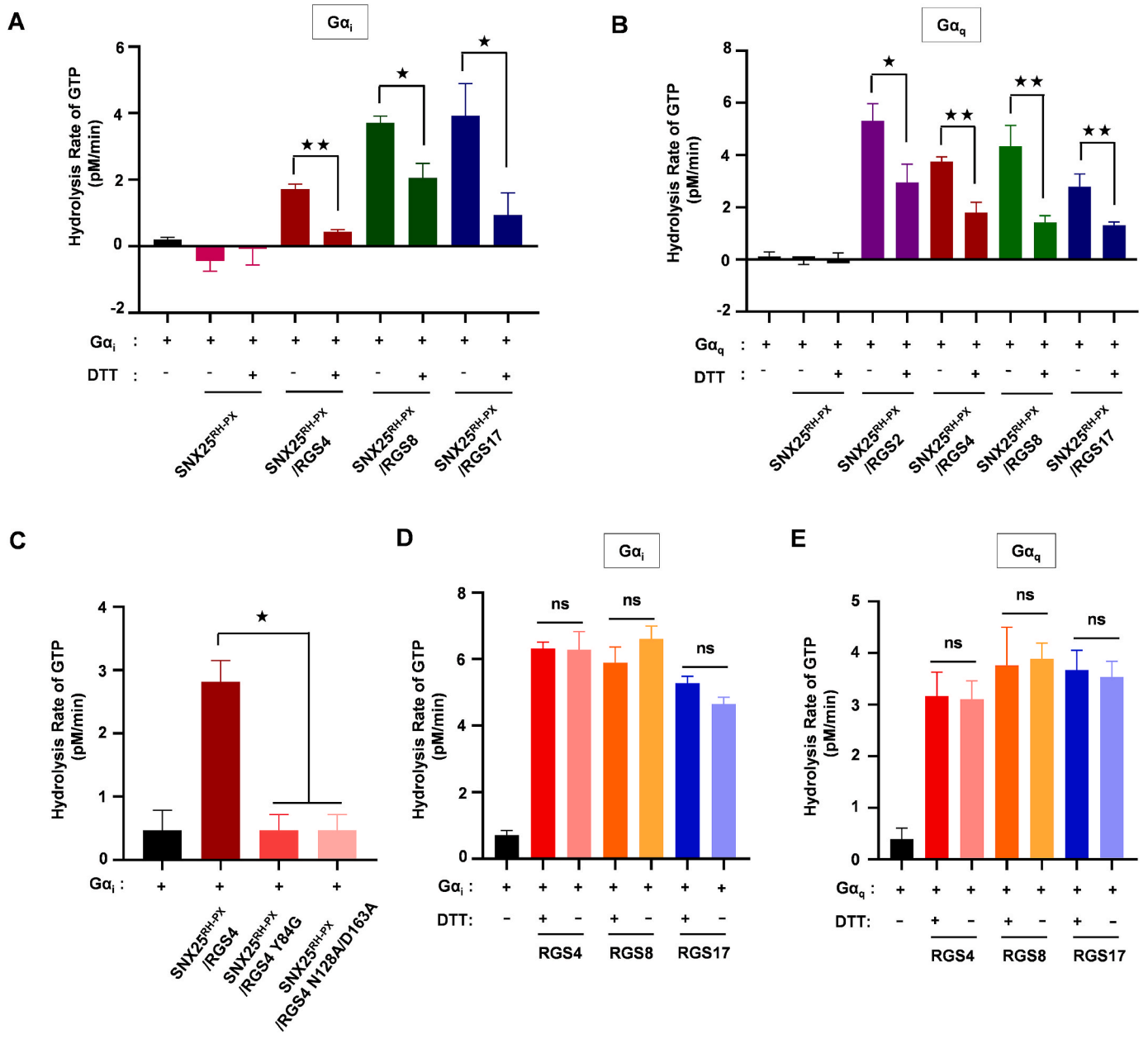

Fig. 5. SNX25 accelerates GAP activity of RGS2, RGS4, RGS8 and RGS17. (A) Effect of mSNX25^{RH-PX}/RGS4 (RGS8 or RGS17) on GTPase activity of $G\alpha_i$ subunit, with or without 5 mM DTT pretreatment. (B) Effect of mSNX25^{RH-PX}/RGS2 (RGS4, RGS8 or RGS17) on GTPase activity of $G\alpha_q$ subunit, with or without 5 mM DTT pretreatment. (C) Determination the GAP activity of mSNX25^{RH-PX}/RGS4 mutant. (D–E) Determination the GAP activity of RGS4, RGS8 and RGS17 toward $G\alpha_i$ (D) or $G\alpha_q$ (E) subunit. Data represents mean from n = 3 experiments, Error bars represent SEM, ns represents no significance ($P > 0.05$). ⋆ $P < 0.05$, ⋆⋆ $P < 0.01$, ⋆⋆⋆ $P < 0.001$ by unpaired student's *t*-test.

SNX25/RGS complex is dependent on the RGS protein itself.

To further investigate the contribution of mSNX25^{RH-PX} to the GAP activity of the complex formed with canonical RGS proteins, we pretreated the complex with 5 mM DTT to disrupt its assembly before subjecting it to the GTPase assay. As shown in Fig. 5A and B, the GAP activity of these complexes towards the $G\alpha_i$ or $G\alpha_q$ subunit was significantly decreased after DTT pretreatment. However, for RGS4, RGS8, and RGS17 that were expressed in HEK293F cells, their GAP activity was not significantly affected by DTT pretreatment (Fig. 5D–E). Unfortunately, we were unable to obtain enough RGS2 protein from HEK293F cells for the GAP activity assay, due to its low expression level. To overcome this limitation, we purified bacterial-expressed RGS proteins (RGS2, RGS4, RGS8, and RGS17). Consistently, DTT pretreatment did not significantly reduce the GAP activity of these purified RGS proteins (Figs. S10B–C). Furthermore, the GAP activity of RGS4 cannot be impaired by mutating C12 or all the four cysteine residues on N-terminal domain (Figs. S10D–E). These results indicate that the GAP activity of these RGS proteins is promoted by the formation of a complex with SNX25.

2.6. SNX25 regulates $G\alpha_i$ -coupled GPCR signaling from endosomes and the plasma membrane

To confirm the role of SNX25 as a regulator of $G\alpha_i$-coupled GPCR signaling, we performed a real-time assay of intracellular cAMP accumulation in HEK293T cells expressing the $G\alpha_i$-coupled D2 dopamine receptor (DRD2), a well-characterized GPCR that mediates the inhibition of adenylyl cyclases (ACs) in response to quinpirole stimulation [27]. By knocking down the endogenous SNX25, we observed a

prominent inhibition of cAMP accumulation in cells treated with ACs activator forskolin and the DRD2 agonist quinpirole (Fig. 6A, Fig. S11A, and Figs. S12A–B). Importantly, the accumulation of cAMP could be rescued by the introduction of exogenous mSNX25 but not by the mSNX25C566A mutant. These results indicate that SNX25 regulates $G\alpha_i$-coupled DRD2 signaling.

To further test the hypothesis that SNX25 regulates GPCR signaling through cooperation with canonical RGS proteins, we analyzed the accumulation of cAMP in HEK293T cells expressing DRD2 along with exogenous mSNX25 and/or RGS proteins (RGS4, RGS8, or RGS17). Due to the low expression level of full-length Flag-tagged mSNX25, we used an mSNX25 fragment with the PXC domain deletion ($mSNX25^{\Delta PXC}$) that retains endosomal targeting ability in this assay (Fig. S9C). Upon treatment with ACs activator forskolin and the DRD2 agonist quinpirole, the cAMP level rapidly accumulated in control cells or cells expressing RGS proteins (Fig. 6B–D). As expected, overexpression of $mSNX25^{\Delta PXC}$ resulted in a significantly increased cellular cAMP accumulation in cells with or without overexpressed RGS proteins. In contrast, the up-regulated cAMP accumulation activity of $mSNX25^{\Delta PXC}$ was almost abolished by mutating C566 to alanine (Fig. 6B–D, Figs. S11B–D, and Figs. S12C–E). Since C566 is essential for SNX25 binding to RGS proteins (RGS4, RGS8, or RGS17), these findings suggest that the regulation of $G\alpha_i$-coupled DRD2 signaling by SNX25 is dependent on its interaction with these canonical RGS proteins.

In our study, we have demonstrated that SNX25 can recruit canonical RGS proteins (RGS4, RGS8, or RGS17) to endosomes (Fig. 4G and Fig. S9B). It is reasonable to examine whether SNX25 regulates GPCR signaling from endosomes. To assess this, we analyzed the expression of two well-characterized endosomal cAMP-dependent genes, phosphoenolpyruvate carboxykinase 1 (*PCK1*) and dapper antagonist of β-catenin, homolog 2 (*DACT2*) [28], in HEK293T cells treated with the β2-adrenoceptor (β2-AR) agonist isoproterenol (Iso) to induce cAMP production. We observed that knockdown of endogenous SNX25 significantly decreased the isoproterenol-induced expression of *PCK1* and *DACT2* in HEK293T cells treated with isoproterenol and quinpirole (Fig. 6E). Consistently, the isoproterenol-induced expression of *PCK1* and *DACT2* could be rescued by overexpressing wild-type mSNX25 but not by expressing the mSNX25C566A mutant (Fig. 6E). These findings indicate that SNX25 promotes the transcription of *PCK1* and *DACT2*. Previous reports have demonstrated that the isoproterenol-induced expression of *PCK1* and *DACT2* can be substantially inhibited by blocking endocytosis using the dynamin inhibitor Dyngo-4a [28], which was confirmed by our qRT-PCR data (Fig. S13). Additionally, our results also showed that SNX25 failed to enhance the expression of *PCK1* and *DACT2* in HEK293T cells treated with Dyngo-4a (Fig. 6E). To investigate whether SNX25 inhibits DRD2 signaling by regulating its endocytosis, we performed immunofluorescence experiments, which revealed that the cellular distribution of DRD2 was not significantly affected by SNX25 knockdown (Fig. S14). These findings indicate that SNX25 regulates cAMP production from endosomes by terminating endosomal $G\alpha_i$ signaling.

To further investigate whether SNX25 rigorously regulates DRD2 signaling from endosomes, we analyzed forskolin-induced cAMP accumulation in the presence of Dyngo-4a treatment. Pretreatment with Dyngo-4a for 30 min resulted in a significant inhibition of DRD2 internalization (Fig. S15A). Interestingly, when cells were treated with Dyngo-4a, the forskolin-induced cAMP accumulation was prominently reduced by knockdown of endogenous SNX25 (Fig. 6F and Fig. S11E). However, this reduction could be rescued by introducing exogenous wild-type mSNX25 but not by the mSNX25 C566A mutant (Fig. 6F and Fig. S11E). Additionally, blocking endocytosis using Dyngo-4a, forskolin-induced cAMP accumulation was also significantly promoted in cells expressing $mSNX25^{\Delta PXC}$ but not in cells expressing the $mSNX25^{\Delta PXC}$ C566A mutant, regardless of the presence or absence of overexpressed RGS proteins (Fig. 6G–I and Figs. S11F–H). These data suggest that SNX25 plays a role in down-regulating $G\alpha_i$-coupled DRD2 signaling from the plasma membrane.

We have previously demonstrated that both the active and inactive forms of $G\alpha_i$ can be recruited to endosomes by mSNX25 in cooperation with canonical RGS proteins. Importantly, strong co-localization of $G\alpha_i$ with RGS4 and SNX25 can be observed in the cytoplasm even after treatment with Dyngo-4a (Fig. S15B). Based on these findings, we propose that in cooperation with canonical RGS proteins, SNX25 not only attenuates signaling of $G\alpha_i$-coupled DRD2 from endosomes, but also regulates its signaling on the plasma membrane by recruiting inactive $G\alpha_i$ to endosomes to prevent its activation on the plasma membrane.

2.7. SNX25 regulates $G\alpha_q$-coupled GPCR signaling from endosomes and the plasma membrane

In addition to regulating $G\alpha_i$-coupled GPCR signaling, SNX25 may also has a role in regulating $G\alpha_q$-coupled GPCR signaling from both endosomes and the plasma membrane. To support this, we used the Bright-Glo™ Luciferase Assay System to assess the signals mediated by overexpressed substance P (SP) neurokinin 1 receptor (NK1R) in HEK293 cells. NK1R is a well-studied $G\alpha_q$-coupled GPCR that is active on both endosomes and the plasma membrane [29]. As shown in Fig. 7A, the luciferase response mediated by NK1R was enhanced by knockdown of endogenous SNX25. Furthermore, in HEK293 cells with knockdown of endogenous SNX25, the NK1R-mediated luciferase level could be reduced by expressing exogenous wild-type mSNX25, but not by expressing the mSNX25 C566A mutant (Fig. 7A and Fig. S16A). Moreover, $SNX25^{\Delta PXC}$ down-regulates the NK1R-mediated luciferase response in SP concentration-dependent manner, both in the presence or absence of overexpressed RGS2 or RGS8 (Fig. 7B–D and Fig. S16B). Importantly, this effect of $SNX25^{\Delta PXC}$ also depends on the C566. These results indicate that SNX25 plays a role in down-regulating $G\alpha_q$-coupled GPCR signaling through cooperation with canonical RGS proteins.

We also investigated the effect of the dynamin inhibitor Dyngo-4a on NK1R internalization and the co-localization of SNX25 with RGS4 and the $G\alpha_q$ subunit. Treatment with Dyngo-4a significantly inhibited NK1R internalization (Fig. S17), but did not alter the co-localization of SNX25 with the $G\alpha_q$ subunit and canonical RGS protein (exampled by RGS4) (Fig. S15B). Interestingly, even in the presence of Dyngo-4a, the NK1R-mediated luciferase level could still be down-regulated by SNX25 in C566 dependent manner (Fig. 7A). These results indicate that, through its interaction with canonical RGS proteins, SNX25 plays a role in regulating $G\alpha_q$-coupled GPCR signaling from the plasma membrane.

It had been reported that nuclear extracellular signal-regulated kinase (ERK) was specifically activated by endosomal NK1R [29]. To investigate whether SNX25 regulates $G\alpha_q$-coupled GPCR signaling from endosomes, we conducted experiments using HEK293T cells expressing the NK1R and a fluorescence resonance energy transfer (FRET) biosensor called NucEKAR, which monitors nuclear ERK activity (Fig. S18). In control cells, stimulation with SP (1 nM) resulted in a sustained activation of nuclear ERK, which was abolished by the dynamin inhibitor Dyngo-4a (Fig. 7E). Interestingly, knockdown of endogenous SNX25 significantly enhanced the SP-induced activation of nuclear ERK (Fig. 7E). Consistently, overexpression of wild-type mSNX25, but not the mSNX25 C566A mutant, reduced the activity of nuclear ERK in SNX25-knockdown cells (Fig. 7E). Furthermore, immunofluorescence experiments revealed that the cellular distribution of NK1R was not significantly altered by knockdown of SNX25, which indicated that SNX25 inhibiting NK1R signaling was not via regulating its endocytosis (Fig. S19). These findings demonstrate that SNX25 is capable of regulating $G\alpha_q$-coupled GPCR signaling from endosomes by acting on the $G\alpha_q$ subunit, in addition to its role in regulating signaling from the plasma membrane.

2.8. Discussion

Increasing evidence have unveiled the significance of G protein

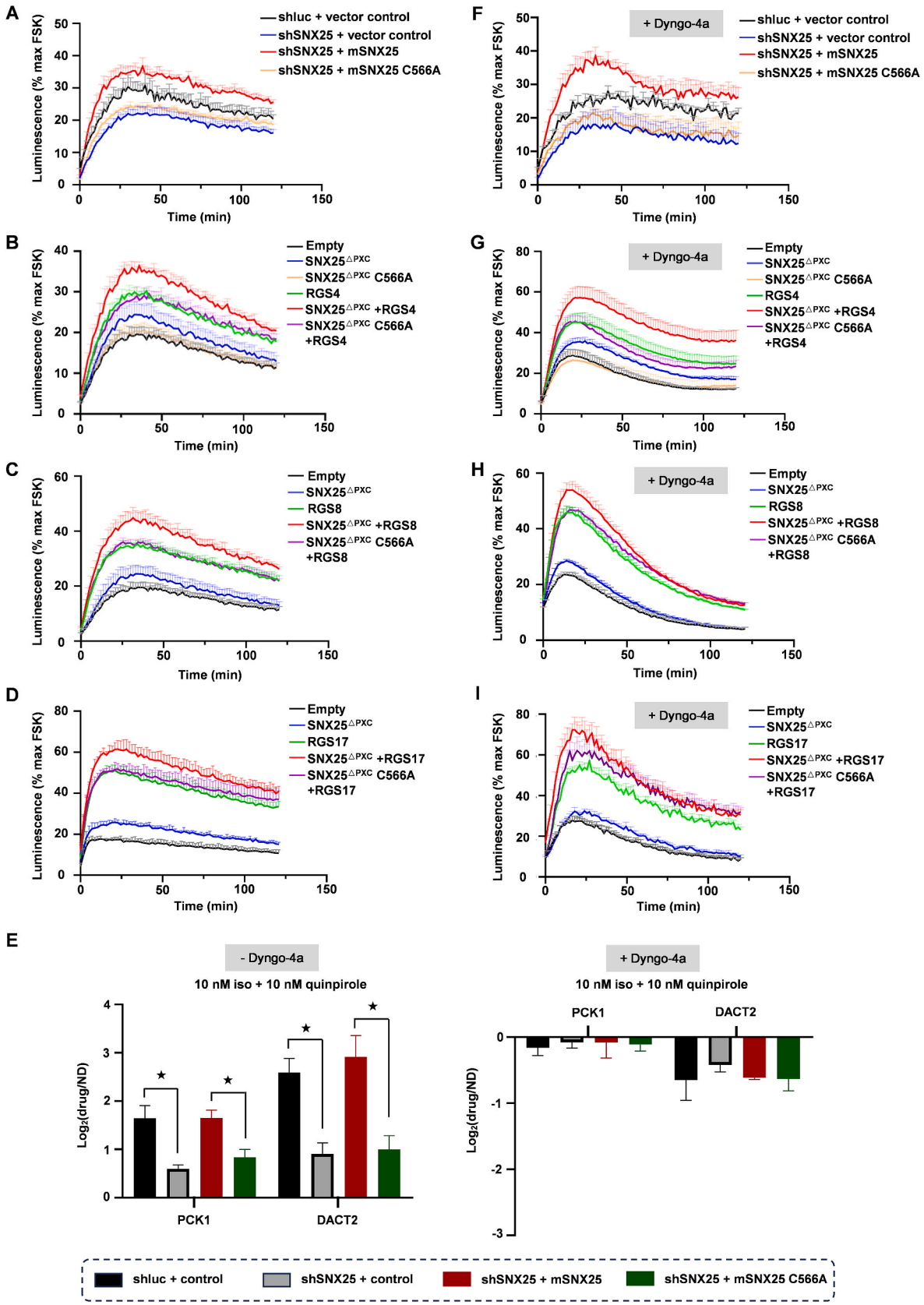

(caption on next page)

Fig. 6. SNX25 regulates GPCR-Gα_i signaling. (A) Effect of endogenous SNX25 on real-time cAMP level in HEK293T cell expressing D2 dopamine receptor (DRD2), in response to quinpirole and forskolin (FSK) treatment. Luminescence was normalized with maximum value in the reference well treated with forskolin (FSK) and DMSO. shSNX25 represents shRNA targeting SNX25, shluc was set as negative control. mSNX25 (WT or C566A mutant) was transfected into the cells expressing shSNX25. (B) Effect of mSNX25$^{\Delta PXC}$/RGS4 on real-time cAMP level in HEK293T cell expressing DRD2, in response to quinpirole and forskolin (FSK) treatment. Luminescence was normalized with maximum value in the reference well treated with forskolin (FSK) and DMSO. (C) Effect of mSNX25$^{\Delta PXC}$/RGS8 on real-time cAMP level in HEK293T cell expressing DRD2, in response to quinpirole and forskolin (FSK) treatment. (D) Effect of mSNX25$^{\Delta PXC}$/RGS17 on real-time cAMP level in HEK293T cell expressing DRD2, in response to quinpirole and forskolin (FSK) treatment. (E) RT-qPCR analysis the effect of SNX25 on the expression of *PCK1* and *DACT2* in response to 10 nM isoproterenol and 10 nM quinpirole, in HEK293T cells with DMSO or Dyngo-4a treatment. The endogenous SNX25 was knockdown by shRNA (shSNX25), shluc was set as negative control. mSNX25 (WT or C566A mutant) was overexpressed in SNX25-knockdown cells. Drug represents isoproterenol and quinpirole treatment. ND, no drug. Iso, isoproterenol. $^{\star}P < 0.05$, $^{\star\star}P < 0.01$ and $^{\star\star\star}P < 0.001$ by unpaired student's *t*-test. (F) Effect of endogenous SNX25 on real-time cAMP level in response to quinpirole and forskolin (FSK) treatment, in DRD2 over-expressed HEK293T cells pretreated with 30 μM Dyngo-4a. (G) Effect of mSNX25$^{\Delta PXC}$/RGS4 on real-time cAMP level in response to quinpirole and forskolin (FSK) treatment, in DRD2 over-expressed HEK293T cells pretreated with 30 μM Dyngo-4a. (H) Effect of mSNX25$^{\Delta PXC}$/RGS8 on real-time cAMP level in response to quinpirole and forskolin (FSK) treatment, in DRD2 over-expressed HEK293T cells pretreated with 30 μM Dyngo-4a. (I) Effect of mSNX25$^{\Delta PXC}$/RGS17 on real-time cAMP level in response to quinpirole and forskolin (FSK) treatment, in DRD2 over-expressed HEK293T cells pretreated with 30 μM Dyngo-4a.

signaling from endosomes [4,5]. However, there is still a gap in understanding how to terminate G protein signaling in the endosome. In this study, we have identified SNX25 as a key player in accelerating the attenuation of Gα_i and Gα_q signaling on endosomes through its interaction with canonical RGS proteins, such as RGS2, RGS4, RGS8, and RGS17, via its PX domain. Additionally, SNX25 forms a complex with these canonical RGS proteins to inhibit GPCR-G$\alpha_{i/q}$ signaling on the plasma membrane. Interestingly, our results further uncover that the termination of G protein signaling through the cooperation of SNX25 and canonical RGS proteins is controlled by redox reactions, implying the importance of redox regulation in the precisely controlled physiological processes mediated by GPCRs.

It has been proposed that SNX proteins, including SNX13, SNX14, and SNX25, with an additional RGS homology domain, possess the potential for G protein signaling termination along with membrane trafficking. While the RGS homology domains of SNX13 and SNX14 have been suggested to act as negative modulators of Gα_s signaling by interacting with the activated Gα_s subunit [16,17], these findings have not been consistently reproduced by other laboratories [13]. Furthermore, our recently published results also demonstrated that the RGS homology domain of SNX25 does not bind to G proteins [18]. Here, we reveal that SNX25, through its PX domain rather than the RGS homology domain, can modulate Gα_i and Gα_q signaling in conjunction with canonical RGS proteins.

The PX domain is a well-known phosphoinositide-binding domain. Studies published previously [21] and presented here clearly demonstrate that the PX domain of SNX25 is non-canonical and cannot bind to phosphoinositides in the conventional manner, due to the absence of conserved residues in the traditional phosphoinositide-binding pocket. In addition to its established role in phosphoinositide recognition, an increasing body of evidence suggest that some PX domains also function as protein-protein interaction modules in membrane trafficking and signaling events [14]. Interestingly, PX domains have been found to interact with diverse binding partners. For example, the PX domain of PLD2 recognizes the SH3 domain of phospholipase C-γ1 through the proline-enriched loop between α1 and α2 [30], and the PX domain of SNX5 binds to IncE via a groove formed by an extended helix insertion and an adjacent β-sheet [31,32]. In this study, we demonstrate that, contrary to previously reported mechanisms, the PX domain of SNX25 interacts with canonical RGS proteins through the formation of an intermolecular disulfide bond, and this interaction can be disrupted by a reducing agent. Thus, our findings provide a novel mechanism for the redox-regulated interaction of the PX domain with protein partners.

Redox dysregulation is implicated in the development of various diseases, including inflammation, cardiovascular disease, and cancer [33,34]. Reactive oxygen species (ROS), as active messengers, can activate several signaling pathways, such as PI3K/AKT/mTOR, MAPKs, and JAK/STAT, which promote cell proliferation [34,35]. Excessive production of ROS can lead to the over-activation of these signaling pathways, contributing to the initiation and progression of leukemia [35]. G protein-coupled receptors (GPCRs), the largest and most druggable membrane receptor superfamily, have also been implicated in redox signaling. Emerging evidence suggest that redox homeostasis plays a crucial role in GPCR signaling. For instance, in astroglioma cells, the cellular redox state modulates Ca^{2+} homeostasis mediated by Gα_q-linked GPCRs [36]. In this study, we provide another example of redox modulation of GPCR signaling. Our results demonstrate that the redox state is critical for SNX25 in regulating G$\alpha_{i/q}$-linked GPCR signaling from endosomes and the plasma membrane. Investigating how redox controls signaling pathways, particularly GPCR signaling, not only helps us understand the mechanisms of cellular signaling regulation under normal and pathological conditions, but also provides opportunities to develop potent strategies against diseases.

It has been well-established that canonical RGS proteins only associate with the active form (GTP-bound) of the Gα subunit. Interestingly, our results demonstrate that, through the formation of a redox-regulated complex with SNX25, canonical RGS proteins, including RGS2, RGS4, RGS8, and RGS17, not only acquire accelerated GTPase-activating protein (GAP) activity but also gain the capacity to bind to the inactive form (GDP-bound) of the Gα subunit. Based on these findings, we propose a mechanism by which SNX25 regulates GPCR-G$\alpha_{i/q}$ signaling (Fig. 8). Under reducing conditions, SNX25 fails to form a complex with canonical RGS proteins, resulting in the loss of its regulatory activity on GPCR-G$\alpha_{i/q}$ signaling. Conversely, under oxidizing conditions, SNX25 forms a complex with canonical RGS proteins. Since SNX25 is localized on early endosomes, the SNX25/canonical RGS complex facilitates the transition of active G$\alpha_{i/q}$ to the inactive form on the endosome, thereby terminating GPCR-G$\alpha_{i/q}$ signaling from endosomes. Additionally, the SNX25/canonical RGS complex can also recruit inactive G$\alpha_{i/q}$ to endosomes, preventing GPCR-mediated activation of G$\alpha_{i/q}$ on the plasma membrane. Consequently, the SNX25/canonical RGS complex negatively regulates GPCR-G$\alpha_{i/q}$ signaling from both endosomes and the plasma membrane.

There is a growing body of evidence indicating the relevance of GPCR signaling from endosomes in various physiological and pathophysiological processes. For example, the activation of the parathyroid hormone receptor (PTHR) endosomal signaling pathway is crucial for skeletal homeostasis [6]. Inhibition of calcium-sensing receptor (CaSR) signaling from endosomes can lead to hypercalcemia [7]. Additionally, endosomal signaling of the glucagon-like peptide-1 receptor (GLP-1R) [8] has been implicated in diabetes, while endosomal signaling of protease-activated receptor 2 (PAR2) [9] has been associated with irritable bowel syndrome. These findings highlight the importance of maintaining homeostasis in GPCR signaling from endosomes for normal physiological functions. Our findings provide valuable insights into the termination of G protein signaling by SNX25 through its complex formation with canonical RGS proteins. This discovery holds promise in the development of potent drugs that target the endosomal GPCR-G signaling pathway.

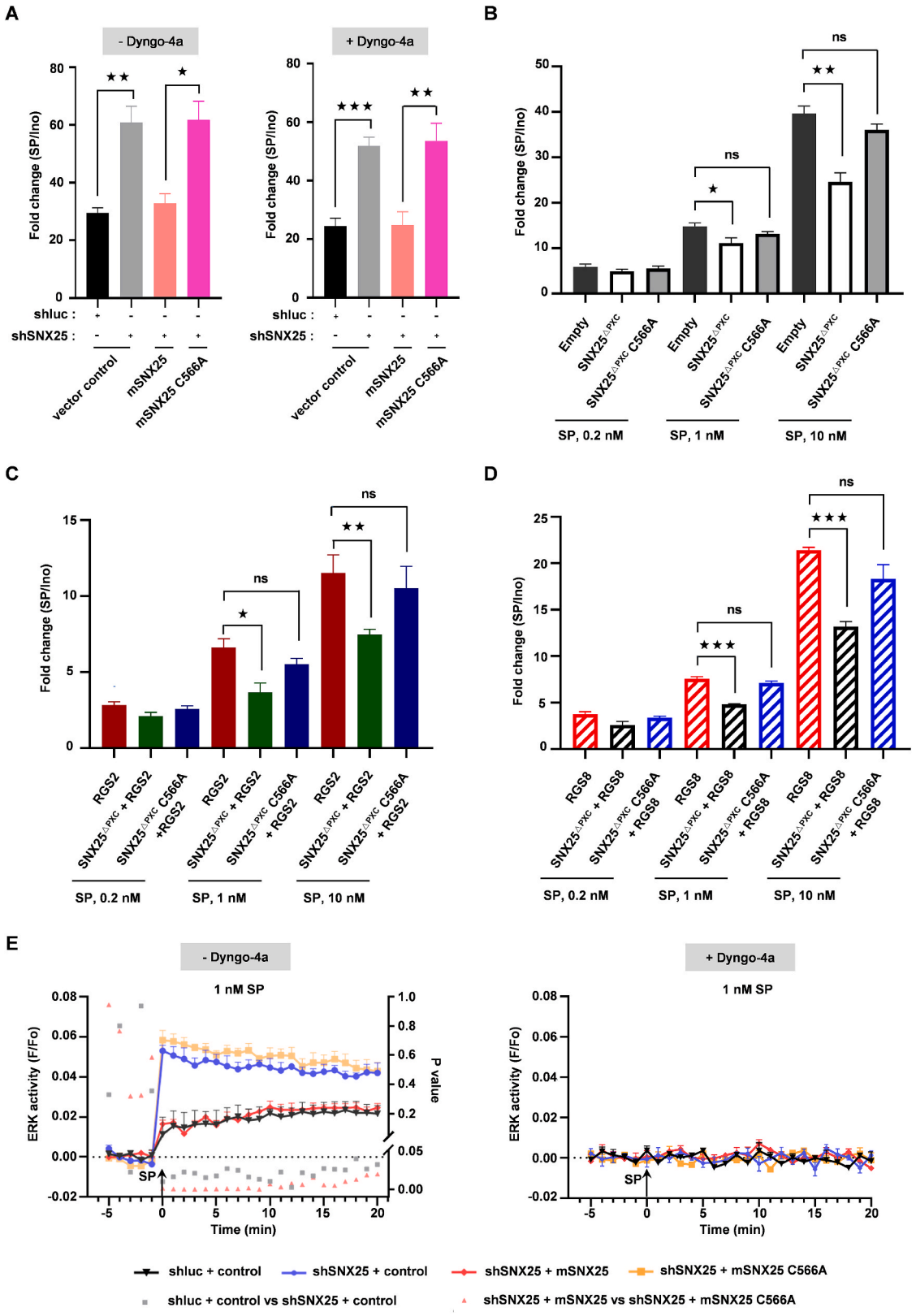

Fig. 7. SNX25 regulates GPCR-Gα_q signaling. (A) Effect of endogenous SNX25 on signaling of over-expressed substance P (SP) activated neurokinin 1 receptor (NK1R) in response to 10 nM SP, in cells pretreated with DMSO or 30 μM Dyngo-4a. (B) Effect of mSNX25$^{\Delta PXC}$ on NK1R signaling in HEK293T cells, in response to bath application of SP with concentration of 0.2 nM, 1 nM or 10 nM. (C–D) Effect of mSNX25$^{\Delta PXC}$ on NK1R signaling in HEK293T cells over-expressing RGS2 (C) or RGS8 (D), in response to bath application of SP with concentration of 0.2 nM, 1 nM or 10 nM. Luminescence was normalized with value in the reference well treated with 1 μM ionomycin (Ino). (E) FRET sensors analysis the effect of SNX25 on the nuclear ERK activity in response to 1 nM SP, in HEK293T cells treatment with DMSO or dyngo-4a. The endogenous SNX25 was knockdown by shRNA (shSNX25), shluc was set as negative control. mSNX25 (WT or C566A mutant) was overexpressed in SNX25-knockdown cells. Data represents mean from n = 3 experiments, Error bars represent SEM, ns represents no significance ($P > 0.05$). $^{\star}P < 0.05$, $^{\star\star}P < 0.01$ and $^{\star\star\star}P < 0.001$, by unpaired student's *t*-test.

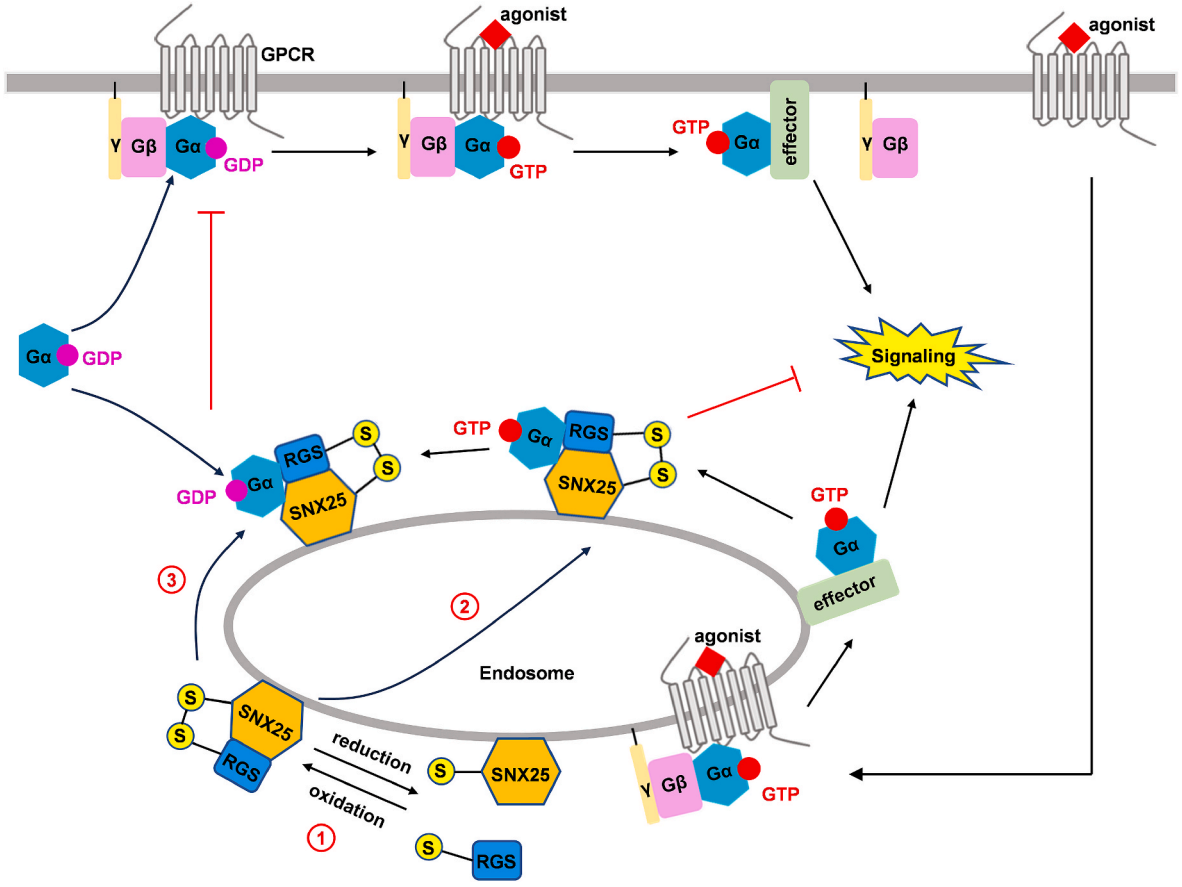

Fig. 8. Proposed mechanisms on redox controlling SNX25 regulation $G\alpha_{i/q}$-coupled GPCR signaling. (1) SNX25 forms redox regulated complex with canonical RGS proteins on endosomes, such as RGS2, RGS4, RGS8 and RGS17, via intermolecular disulfide bond. (2) SNX25/RGS protein complex binds to activated $G\alpha_{i/q}$ on endosomes, and accelerates its GTPase activity, thus terminating $G\alpha_{i/q}$ signaling from endosomes. (3) SNX25/RGS protein complex can recruit GDP-bound $G\alpha_{i/q}$ to endosomes, preventing $G\alpha_{i/q}$ activation by GPCR on the plasma membrane.

3. Methods

3.1. Molecular cloning

The molecular cloning procedures were performed using standard techniques. The accession numbers of the mouse SNX25 (mSNX25), RGS2, RGS4, RGS8, and RGS17 used in this study were NP_997096.2, NP_002914.1, NP_005604.1, NP_203131.1, and NP_036551.3, respectively.

For bacterial expression of mSNX25-PX, the cDNA encoding the PX domain of mSNX25 (residues 506–624) was cloned into the pET21a vector with a C-terminal 6 × His tag. To investigate the interaction between mSNX25 and RGS proteins (RGS2, RGS4, RGS8, and RGS17) using Co-IP, various domains of mSNX25 were cloned into the pcDNA3.1 vector with a Flag tag at the N-terminus. The cDNAs encoding RGS2, RGS4, RGS8, and RGS17 were cloned into the pcDNA3.1 vector with a HA tag at the C-terminus. To assess the importance of the N-terminal domain for the interaction between RGS proteins and mSNX25, the cDNAs encoding $RGS2^{\Delta N}$ (residues 72–211), $RGS4^{\Delta N}$ (residues 51–205), $RGS8^{\Delta N}$ (residues 45–180), and $RGS17^{\Delta N}$ (residues 73–210), as well as the full-length versions of RGS2, RGS4, RGS8, and RGS17, were cloned into the pcDNA3.1 vector with a Flag tag at the N-terminus, respectively. The cDNA encoding the RH-PX domain of mSNX25 (residues 280–624) was subcloned into the pcDNA3.1 vector with a HA tag at the C-terminus. To examine the interaction between the mSNX25/RGS protein complex and $G\alpha_{i/q}$ subunits, the cDNAs encoding $G\alpha_{i/q}$ subunits were cloned into the pcDNA3.1 vector with a HA tag at the C-terminus.

For the luciferase reporter assay involving mSNX25, the cDNA encoding $mSNX25^{\Delta PXC}$ (residues 1–624) was cloned into the pcDNA3.1 vector with a Flag tag at the N-terminus. For fluorescence colocalization experiments, the PX (residues 506–624) or RH-PX (residues 280–624) domain of mSNX25 was cloned into the pcDNA3.1 vector with a GFP tag at the C-terminus. Additionally, the PXA (residues 1–279), PXC (residues 625–840), and full-length mSNX25 were cloned into the pcDNA3.1 vector with a GFP tag at the N-terminus. The two FYVE domains derived from the tandem FYVE domain of HGS (residues 147–223) linked by the linker QGQGS were cloned into the pcDNA3.1 vector with a dsRed tag at the N-terminus. The RGS proteins, including RGS2, RGS4, RGS8, and RGS17, were cloned into the pCDNA3.1 vector with a dsRed or mCherry tag at the C-terminus. The cDNAs encoding Gα subunits, including $G\alpha_i$, $G\alpha_q$, and $G\alpha_s$, were cloned into the pcDNA3.1 vector with a Flag or CFP tag at the C-terminus. Site-directed mutants were generated following the site-directed mutagenesis protocol.

3.2. Co-immunoprecipitation (Co-IP)

To determine the interaction of over-expressed proteins, HEK293T cells were cultured in 10 cm dishes until reaching 70%–80 % confluency prior to gene transfection. For transfection, 10 μg of plasmid DNA was mixed with 50 μL of PEI (Polyethylenimine, Polysciences). After 48 h of transfection, cells were collected and washed with PBS. The collected cells were lysed in 500 μL of lysis buffer (50 mM Tris pH 8.0, 150 mM KCl, 1 mM EDTA, 5 % glycerol, 1 % NP40) supplemented with a protease inhibitor cocktail (Roche) and PMSF, and incubated at 4 °C for 30 min. The cell lysates were then clarified by centrifugation at 4 °C, 12,000 rpm for 20 min. The concentration of the supernatant was determined using a

BCA kit. Next, 20 μL of Flag resin, which had been washed with IP buffer (50 mM Tris pH 8.0, 150 mM KCl, 5 % glycerol) three times, was added to a mixture containing 1 mg of total protein from the supernatant and 600 μL of IP buffer. The mixture was incubated overnight at 4 °C. The resin was then washed three times with IP washing buffer (50 mM Tris pH 8.0, 150 mM KCl, 5 % glycerol, 0.1 % NP40) and subsequently eluted with 120 μL of 3x Flag peptide for 2 h. The eluent was analyzed by western blotting to detect the interacting proteins.

To determine the interaction of endogenous proteins in IMR-32 cells, about 6×10^7 cells were lysed in 3 mL lysis buffer supplemented with a protease inhibitor cocktail (Roche) and PMSF. The cell lysates were then clarified by centrifugation at 4 °C, 12,000 rpm for 20 min. Then, 2 μg anti-SNX25 antibody (Rabbit, Proteintech) or the negative control IgG antibody (Rabbit, CST 2729S) was added to mixture containing 1 mL supernatant and 2 mL IP buffer. After incubation overnight at 4 °C, 15 μL Protein A and 15 μL Protein G resin (Invitrogen), which had been washed with IP buffer three times, was added to mixture for 3 h. The resin was then washed three times with IP washing buffer. Then, the resin was mixed with loading buffer. After heated for 10 min at 100 °C, the sample was analyzed by western blotting to detect the interacting proteins.

3.3. Western blotting

The protein samples were separated by SDS-PAGE (sodium dodecyl sulfate-polyacrylamide gel electrophoresis) and transferred onto PVDF membranes. The membrane was then blocked with 5 % skim milk dissolved in TBST buffer (20 mM Tris-HCl pH 8.0, 150 mM NaCl, 0.05 % (v/v) Tween 20) for 1 h at room temperature to prevent non-specific binding. Next, the membrane was incubated with the primary antibody, either anti-Flag antibody (1:1000, mouse, Beyotime Biotechnology), anti-HA antibody (1:2000, rabbit, abcam ab9110), anti-RGS4 antibody (1:1000, mouse, Proteintech) or anti-$G\alpha_i$ antibody (1:1000, mouse, Proteintech) diluted in TBST buffer containing 5 % skim milk, overnight at 4 °C. Afterwards, the membrane was washed with TBST buffer three times to remove any unbound antibody. The membrane was then incubated with the appropriate secondary antibody conjugated with horseradish peroxidase (HRP), either anti-mouse secondary antibody (1:1000, Cell Signaling) or anti-rabbit secondary antibody (1:5000, Abkine A25222), for 2 h at room temperature. Following another round of washing with TBST buffer three times, the membrane was developed using a chemiluminescence developer (Life Science) to visualize the protein bands. The chemiluminescent signal could be captured on an X-ray film or detected using a chemiluminescence imaging system.

3.4. Mass spectrometry-based protein identification

To perform mass spectrometry-based protein identification, the protein solution obtained from the co-IP was first diluted to 300 μL using UA solution (8 M urea in 0.1 M Tris-HCl, pH 8.5). The solution was then reduced by adding 50 mM DTT and incubating at 37 °C for 1 h. The reduced solution was discarded by centrifugation at 12,000 g for 15 min. Next, the protein was dissolved in UA solution containing iodoacetamide (IAA) in the dark for 30 min at room temperature. The protein solution was then loaded onto a filter tube and rinsed with 200 μL of UA solution twice, followed by rinsing with 200 μL of TEAB (50 mM triethylammonium bicarbonate) five times. The filter tube was centrifuged at 12,000 g for 12 min at room temperature to collect the protein.

For protein digestion, 100 μL of TEAB containing 2 μg of Trypsin Gold (Promega, USA) was added to the protein on the filter tube, and the digestion was performed at 37 °C for 18 h. The resulting peptides were collected by centrifugation at 12,000 g for 15 min and then lyophilized. The peptides were desalted using a MonoTip C18 column (GL Sciences) and eluted peptides were freeze-dried and stored at −20 °C until LC-MS analysis.

The LC-MS/MS detection system used was the Orbitrap Q Exactive HF-X mass spectrometer (Thermo Fisher, USA). A 1.0 μg mixture of peptides was dissolved in buffer A (0.1 % formic acid) and loaded onto a 2-cm trap column (75-μm inner diameter, Acclaim PepMap 100 C18, 3 μm, Thermo Scientific) using buffer A. The peptides were then separated on a 75-μm-inner-diameter column with a length of 25 cm (Acclaim PepMap 100C18, 2 μm; Thermo Scientific) over a 60-min gradient. The mass spectrometer was operated in positive-ion mode at an ion transfer tube temperature of 320 °C and a positive-ion spray voltage of 3.7 kV. The full mass spectrometry survey scan resolution was set to 60,000 with an automated gain control (AGC) target of 3×10^6. The scan range was set from 350 to 1800 m/z with a maximum injection time of 50 ms. Fragmentation of peptides was performed using higher-energy collision dissociation (HCD) at a normalized collision energy of 28 %. The AGC target for MS2 was set to 1×10^5 with a maximum injection time of 30 ms, and a dynamic exclusion time of 60 s was applied.

The resulting tandem mass spectra were then searched against the *Homo sapiens* (Human) UniProt database (9606) using Proteome Discoverer software (version 2.3, Thermo Scientific) and the Basic_Sequest™ HT search engine. Trypsin was selected as the proteolytic enzyme, allowing for two missed cleavage sites. Cysteine carbamidomethylation was set as the fixed modification, while oxidation of methionine (M) and acetylation of the protein N-terminus were set as variable modifications. The search mass tolerance was set to 10 ppm. The false discovery rates (FDR) for peptide-spectrum matches (PSMs) and proteins were both set to less than 1 %.

3.5. Protein expression and purification

For bacterial expression, the PX domain of mSNX25, RGS proteins (including RGS2, RGS4, RGS8 and RGS17) and $G\alpha_i$ subunit were expressed in *Escherichia coli* Rosetta 2. Cells were grown in LB medium at 37 °C for about 3 h until OD_{600} up to 0.6–0.8. Expression was induced with 0.5 mM IPTG, and further cultured at 16 °C for 20 h. Bacteria was collected by centrifugation at 5000 rpm for 10 min and resuspended in lysis buffer (20 mM Tris pH 8.0, 300 mM NaCl, 5 % glycerol, 7 mM β-mercaptoethanol (β-ME)). The cell was lysed by high pressure homogenizer and then centrifuged, 12,000 rpm for 30 min at 4 °C. The supernatant was then loaded onto Ni affinity column (Qiagen, Hilden, Germany), the target protein was eluted with buffer containing 20 mM Tris-HCl pH 8.0, 300 mM NaCl, 300 mM imidazole, 7 mM β-ME. The eluted protein was further purified by gel filtration (Hiload 16/60 Superdex 75 column), equilibrated against buffer containing 20 mM Tris pH 7.5, 100 mM NaCl, 5 mM dithiothreitol (DTT).

To obtain the dimer form SNX25-PX, 100 μM purified mSNX25-PX monomer was oxidized by 500 μM H_2O_2 for 30 min at 16 °C. Then, the oxidized mSNX25-PX dimer was separated by gel filtration (Superdex™ 75 Increase). To transform the oxidized dimer to monomer, the oxidized dimer of SNX25-PX was treated by 5 mM DTT for 30 min at 16 °C, was and then purified by gel filtration (Superdex™ 75 Increase).

To obtain the complex of $mSNX25^{RH-PX}$ with RGS protein, including RGS2, RGS4, RGS8 or RGS17, Flag-tagged $mSNX25^{RH-PX}$ and HA-tagged RGS proteins were co-expressed in 293F cells, respectively. When the cell density reaches to 4×10^6, the plasmids of $mSNX25^{RH-PX}$-Flag and RGS2-HA (RGS4-HA, RGS8-HA or RGS17-HA) were co-transfected with ratio of 1:1. After 72 h of transfection, cells were collected by centrifugation at 2000g for 5 min and resuspended in lysis buffer (20 mM Tris pH 7.5, 150 mM NaCl) with protease inhibitor cocktail (Roche) and PMSF. The cell was lysed by high pressure homogenizer and then centrifuged at 12,000 rpm for 60 min at 4 °C. The Flag resins (GenScript) were incubated with supernatant for 2 h and washed with lysis buffer for 10 column volumes. The targeted proteins were eluted by elution buffer (20 mM Tris pH 7.5, 150 mM NaCl, 125 μg/mL 3 × Flag peptides). The proteins of RGS4, RGS8, RGS17 and $G\alpha_q$ subunit were expressed in 293F cells and purified by Flag resins with the same manner as the complex of $mSNX25^{RH-PX}$ with RGS protein.

3.6. Crystallization, data collection and structure determination

For crystallization, the PX domain of mSNX25 eluted from gel filtration was further concentrated to 9.8 mg/mL by ultrafiltration (Millipore Amicon). Crystallization was performed using sitting drop vapor diffusion method by mixing protein with reservoir solution at volume ratio 1:1. Crystal of SNX25 PX domain was grown at 293 K with reservoir solution containing 1.8 M Magnesium sulfate hydrate, 0.1 M Sodium acetate trihydrate pH 4.8.

To improve crystal quality, crystal dehydration was performed by soaking crystal in mother liquid with addition of 30 % PEG400 for 48 h. All crystals were cryoprotected in mother liquid with addition of 30 % glycerol before collecting diffraction data at 100K. Diffraction data was collected at Beam Line 19U1 (BL19U1) [37] of National center for Protein Science (Shanghai) and the Shanghai Synchrotron Radiation Facility. Diffraction data was processed with Mosflm [38], and scaled with Aimless [39]. Crystal structure was solved by molecular replacement using Molrep [40] with starting model of PX domain of zebrafish SNX25 (PDB code 5XDZ). Buccaneer [41] and coot were used to complete model building. Refinement of the structure was conducted with Refmac 5 [42]. Data collection and refinement statistics are shown in Supplementary Table 1.

3.7. Subcellular localization assay

Hela cells were grown on coverslips placed in 12-well plate. Plasmid (1 μg) was transfected into cells, when the cell density reached 50 %. After 40 h of transfection, the cells were washed with PBS three times, then fixed with 4 % PFA for 20 min at room temperature, subsequently penetrated and blocked with 0.2 % Triton X-100 and 3 % BSA for 1 h, at room temperature. To visualize Flag or HA-tagged protein, the cells were incubated with anti-Flag antibody (1:100, Rabbit, Beyotime Biotechnology) or anti-HA antibody (1:500, Rabbit, abcam ab9110) at 4 °C overnight, after washed with PBS for three times. The cells were further incubated with anti-Rabbit antibody conjugated with Alexa Fluor™ 647 (1:400, Invitrogen, A21244) for 1 h at room temperature. Then, cells were incubated with DAPI (1:2000, Sigma-Aldrich, D9542) for 1 min. Finally, the coverslips were mounted on the slides by antifade mounting medium (VECTASHIELD) prior to observation through confocal microscope (Leica SP8 X STED). To observe DAPI, CFP, GFP, dsRed (or mCherry) and Alexa Fluor™ 647, the excitation wavelength was set to 405 nm, 451 nm, 488 nm, 561 nm and 647 nm, respectively. Meantime, to avoid excitation light interference, the collecting wavelength was 10 nm away from excitation wavelength. To assess the reproducibility of the colocalization, the lower-magnification widefield images were collected. Co-localized cells were counted, and statistical significance was analyzed according to unpaired student's t-test.

3.8. Disulfide bond identification by mass spectrometry-based proteomics

The purified proteins derived from Co-IP were alkylated by 15 mM iodoacetamide at room temperature in the dark for 45 min to block the free sulfhydryl group. Then, the alkylated proteins were digested by trypsin at 37 °C overnight. The tryptic peptides were acidified to pH < 2 by trifluoroacetic acid and loaded into homemade C18 StageTips (Supelco, 66883-U) for desalting. Desalted peptides were separated and analyzed with an Easy-nLC 1200 (Thermo Fisher Scientific) connected online to Fusion Lumos mass spectrometer equipped with FAIMS pro (ThermoFisher Scientific).

Tryptic peptides were separated at a flow rate of 600 nL/min with a linear gradient of 2 %–5 % mobile phase B (0.1 % formic acid and 20 % acetonitrile in water, v/v) within 2 min, followed by a linear increase from 5 % to 36 % mobile phase B within 98 min and 36 %–45 % mobile B within 12 min, then an 8 min plateau before re-equilibration. Survey full-scan MS spectra (from m/z 300 to 1500) were acquired in the Orbitrap with resolution r = 120,000. The automated gain control (AGC) was set as 2×10^5 charges and the maximum injection time was set as 50 ms. The ions were selected for fragmentation in higher-energy collisional dissociation (HCD) with 30 % collision energy. Fragment ion spectra were acquired in the Orbitrap mass analyzer with an AGC of 1×10^4 and a maximum injection time of 22 ms was set for MS2 detection. The isolation window was set as m/z 1.6, and the number of selected precursor ions with a charge state 3^+ to 5^+ was determined by the "Top Speed" acquisition algorithm with a dynamic exclusion of 80 s and 10 p.p.m.

The raw files were further analyzed by pLink 2 algorithm version 2.3.9 [43] searching against targeted proteins, including mSNX25, RGS2, RGS4, RGS8 and RGS17. The flow type was set as Disulfide Bond (HCD-SS) and the linker was set as disulfide. Nethylmaleimide (C) and Carbamidomethyl (C) were set as the variable modifications. The results were visualized by pLabel version 2.4 [44].

3.9. GTPase activity assay

GTPase activity of $G\alpha_{i/q}$ was measured using the ATPase/GTPase Activity Assay Kit (MAK-113, Sigma-Aldrich) according to the manufacturer's instruction. The protein of $G\alpha_{i/q}$ was diluted to 10 μM with assay Buffer (20 mM Tris pH 7.5, 150 mM NaCl, 500 μM GTP, 5 mM $MgCl_2$). To check the GAP activity of RGS proteins in complex with SNX25, the complexes of $mSNX25^{RH-PX}$-Flag and RGS2-HA (RGS4-HA, RGS8-HA or RGS17-HA) were diluted to 0.5 mg/mL with assay buffer, and mixed with 10 μM $G\alpha_{i/q}$, respectively. For the GAP activity of RGS proteins towards $G\alpha_{i/q}$ subunits, RGS proteins (including RGS2, RGS4, RGS8 and RGS17) were diluted to 0.25 mg/mL with assay buffer, and mixed with 10 μM $G\alpha_{i/q}$, respectively. 20 μL of the reaction mixture was incubated for 1 h at 20 °C in 384 well transparent plates (Corning). For the GAP activity of RGS proteins towards $G\alpha_{i/q}$ subunits, RGS proteins (including RGS2, RGS4, RGS8 and RGS17) were diluted to 0.25 mg/mL with assay buffer, and mixed with 10 μM $G\alpha_{i/q}$, respectively. Then, 80 μL of malachite green reagent was added into each reaction well and incubated for 30 min. After that, the absorbance at 620 nm was measured. Reaction without $MgCl_2$ was set up for background. Statistical significance was analyzed according to unpaired student's t-test.

3.10. Construction shRNA for knockdown SNX25

To knockdown endogenous SNX25, shRNA targeting the CDS region of hSNX25 (5′ GAAGC AACTAAGGTATCAAATCTCGAGATTTGATACCTTAGTTGCTTC 3′) was constructed to pLKO.1 vector. shluc (5′ CCTAAGGTTAAGTCGCCCTCGCTCGAGCGAGGGCGACTTAACCTTAGG 3′) targeting luciferase was set as negative control. Constitutive expression of shRNA was performed by lentiviral infection of the pLKO.1 vector with puromycin (2.5 μg/ml) selection. Knock down efficiency was validated by western blot (anti-SNX25, 1:1000, Rabbit, Proteintech) and RT-qPCR. The primers used in qPCR were: forward 5′ CTGCACCACAGACTGAGTCAC 3′ and reverse 5′ TGCAACACAAAAGGTCTTGGC 3′.

3.11. Lentivirus generation and transfection

Lentivirus was obtained from PEI transfection of HEK293T cells by co-transfecting the packing vectors of psPAX2 and pMD2.G along with gene delivery vector (pLKO.1). Viral supernatants were collected by 0.45 μM membrane filtration after 48 h of transfection. For infection, the lentivirus solution was added into cells in the presence of polybrene (8 μg/ml). After 48 h of infection, medium containing the lentivirus was discarded and infected cells was selected by puromycin (2.5 μg/ml).

3.12. Cellular cAMP signaling assays

HEK293T cells were transfected using 10 μL lipofectamine 2000 (Invitrogen) with 4 μg of total plasmids including pGloSensor™-22F cAMP biosensor plasmid (Promega), dopamine D2 receptor,

mSNX25$^{\Delta PXC}$ (wild type or C566A mutant) with N-terminal Flag tag and RGS4-HA (RGS8-HA or RGS17-HA) in six-well plate. For shRNA knockdown endogenous SNX25 assays, the plasmid of full length mSNX25 (WT or C566A) was transfected into the cells of shRNA knockdown endogenous SNX25 along with pGloSensor™-22F cAMP biosensor plasmid and dopamine D2 receptor. Total DNA amount was equilibrated with empty pCDNA3.1 vector. After 24 h of transfection, cells were re-plated to flat-bottom, white 96-well plates at a density of 60,000 cells/well. After 48 h of transfection, culture medium was discarded and washed once with CO_2-independent DMEM medium supplemented with 10 % fetal bovine serum. Then, cells were incubated with 100 μL equilibration medium (assay medium with 4 % GloSensor™ substrate) for 2 h. After 2 h, 20 μL quinpiroles (diluted into 10 μM forskolin containing assay medium) was added to each well in final concentration of 5 μM. To check the cAMP signaling under the condition of endocytosis inhibition, the cells was incubated with 30 μM Dyngo-4a for 30 min before treatment with quinpirole. The plate was subsequently read in microplate reader (BioTek, Cytation 5). Reference wells were treated with 10 μM forskolin and DMSO. Statistical significance was analyzed according to unpaired student's t-test. All the experimental luminescence value was normalized with maximal response in the reference well.

3.13. Gene expression analysis

HEK293T cells were grown in 12-well plate at about 70 % confluency. The 0.3 μg plasmid of mSNX25 (WT or C566A mutant) was transfected into the HEK293T cells with shSNX25, meantime, the corresponding empty vector was transfected into shluc or shSNX25 cells. After 48 h of transfection, the cells were displaced with fresh medium. 30 μM Dyngo-4a or DMSO was added and incubated for 30 min, followed by the addition of 10 nM isoproterenol and 10 nM quinpirole) for 2 h. Total RNA was extracted with Trizol and chloroform, and quantified by nanodrop. 2.5 μg total RNA was used to generate cDNA. Log_2 ratios ('Iso + quinpirole'/'No drug') were calculated. Statistical significance was analyzed according to unpaired student's t-test.

3.14. Reverse transcription quantitative real-time PCR (RT-PCR)

Total RNA was extracted with Trizol and chloroform, and precipitated by isopropanol. Then, total RNA was further washed by 75 % alcohol and 100 % alcohol, respectively. Reverse transcription was carried out with M-MLV reverse transcriptase (Promega) and a mix of oligo (dT) following standard protocols. The generated cDNA was used as input for quantitative PCR with Tag Pro Universal SYBR qPCR Master Mix (Vazyme). Statistical significance was analyzed according to unpaired student's t-test. All gene expression levels were normalized with the levels of the housekeeping gene β-actin.

The qPCR primers for β-actin, *PCK1*, *DACT2* and *mSNX25* were followed:

Gene	Forward	Reverse
β-*actin*	CCTTCCTTCCTGGGCATGG	GATCTTCATTGTGCTGGGTGC
PCK1	AAAACGGCCTGAACCTCTCG	ACACAGCTCAGCGTTATTCTC
DACT2	AGCCGCTGCTTCTACTGGA	GAGGGTGGACTCAGAACAGGA
mSNX25	GGCTTTGCTCACTCACTTCTG	GTACGTAAGCTGAGAGACTGG

3.15. Bright-Glo™ luciferase assay

HEK293T cells were cultured to 70 %–80 % density to conduct gene transfection in six-well plate. 4 μg of plasmids including pGL4.30 Ca^{2+} sensor plasmid (contains an NFAT response element and *luc2P* reporter gene), NK1R (Neurokinin 1 receptor), mSNX25 (wild type or C566A mutant) with N-terminal Flag tag and RGS2-HA (or RGS8-HA) were transfected into cells using 10 μL of lipofectamine 2000 (Invitrogen). After 24 h of transfection, cells were re-plated to, 96-well white flat-bottom plates at a density of 60,000 cells/well. After 42 h of transfection, cells were treated with 0.2 nM, 1 nM and 10 nM substance P (NK1R agonists), respectively. For the control group, cells were treated with 1 μM ionomycin. To check the luciferase signaling under the condition of endocytosis inhibition, the cells was incubated with 30 μM Dyngo-4a for 30 min before treatment with substance P. After 6 h of treatment, cells were rinsed with PBS and subsequently lysed by 30 μL Glo lysis buffer (Promega) for 5 min. Then, Bright-Glo™ assay reagent was added to each well. After incubation for 5 min, bright luminescence was measured using a luminometer (Promega) following the manufactures instructions.

3.16. FRET measurements for endosomal NK1R signaling

HEK293T cells were cultured to 70 %–80 % confluency to conduct gene transfection in six-well plate. Total 2 μg of plasmids including 0.5 μg mSNX25 (wide type or C566A mutants), 0.75 μg NK1R and 0.75 μg FRET sensors (NucEKAR derived from Addgene, plasmid 18,682) were transfected into the SNX25 knockdown cells. The equal amount vector corresponding with mSNX25 was transfected into the control or SNX25 knockdown cells. After 24 h of transfection, cells were re-plated to 96-well black flat-bottom plates at a density of 60,000 cells/well. After 48 h of transfection, FRET for GFP/RFP emission ratio analysis was assessed using PerkinEImer Envision. The cells were sequentially excited using a FITC filter (480/10) with emission measured using RFP (595/30) and FITC (535/20) filters every 1 min. Baseline emission ratio was captured for 5 min, followed by activation with an EC_{50} concentration of substance P (SP, 1 nM) for 20 min. To reveal the NK1R signaling under the condition of endocytosis inhibition, the cells were treated with 30 μM dyngo-4a for 30 min before treatment with substance P. Data was analyzed and expressed as emission ratios relative to baseline (F/Fo). Statistical significance was analyzed according to unpaired student's t-test.

Data availability

Atomic coordinates and structure factors amplitudes for crystal structure of mouse SNX25 PX domain have been deposited into Protein Data Bank with accession code (8HQL).

CRediT authorship contribution statement

Yulong Zhang: Formal analysis, Investigation, Writing – original draft. **Zhijun Yu:** Investigation. **Mingwei Sun:** Investigation. **Ruyue Du:** Investigation. **Hanhan Gao:** Investigation. **Qiankun Dai:** Investigation. **Yan Dong:** Investigation. **Cuicui Liu:** Investigation. **Menghui Yin:** Investigation. **Tingting Xu:** Investigation. **Xiaofei Zhang:** Investigation. **Jinsong Liu:** Project administration, Writing – review & editing. **Jinxin Xu:** Conceptualization, Formal analysis, Investigation, Writing – original draft, Writing – review & editing.

Declaration of competing interest

The authors declare no competing interests.

Acknowledgements

We thank the staff from BL19U1 beamline of National Facility for Protein Science in Shanghai (NFPS) and Shanghai Synchrotron Radiation Facility, for assistance during the diffraction data collection. We thank Professor Xiaodong Shu for providing cDNA of mSNX25, and thank Dr. Wenjing Guo for assistance during fluorescence imaging. The work was financially supported by grant from National Natural Science Foundation of China (32171213), Project of The State Key Laboratory of Respiratory Disease (SKLRD-Z-202009), and Guangdong Provincial Key

Laboratory of Biocomputing (2016B030301007).

Appendix A. Supplementary data

Supplementary data to this article can be found online at https://doi.org/10.1016/j.redox.2024.103253.

The authors declare that they have no known competing financial interests or personal relationships that could have appeared to influence the work reported in this paper.

References

[1] J.P. Mahoney, R.K. Sunahara, Mechanistic insights into GPCR-G protein interactions, Curr. Opin. Struct. Biol. 41 (2016) 247–254.
[2] N.J. Pavlos, P.A. Friedman, GPCR signaling and trafficking: the long and short of it, Trends Endocrinol. Metabol. 28 (2017) 213–226.
[3] N.G. Tsvetanova, R. Irannejad, M. von Zastrow, G protein-coupled receptor (GPCR) signaling via heterotrimeric G proteins from endosomes, J. Biol. Chem. 290 (2015) 6689–6696.
[4] S.E. Crilly, M.A. Puthenveedu, Compartmentalized GPCR signaling from intracellular membranes, J. Membr. Biol. 254 (2020) 259–271.
[5] N. Caengprasath, A.C. Hanyaloglu, Hardwiring wire-less networks: spatially encoded GPCR signaling in endocrine systems, Curr. Opin. Cell Biol. 57 (2019) 77–82.
[6] A.D. White, et al., Spatial bias in cAMP generation determines biological responses to PTH type 1 receptor activation, Sci. Signal. 14 (2021) eabc5944.
[7] C.M. Gorvin, et al., AP2sigma mutations impair calcium-sensing receptor trafficking and signaling, and show an endosomal pathway to spatially direct G-protein selectivity, Cell Rep. 22 (2018) 1054–1066.
[8] R.S. Kuna, et al., Glucagon-like peptide-1 receptor-mediated endosomal cAMP generation promotes glucose-stimulated insulin secretion in pancreatic beta-cells, Am. J. Physiol. Endocrinol. Metab. 305 (2013) E161–E170.
[9] N.N. Jimenez-Vargas, et al., Protease-activated receptor-2 in endosomes signals persistent pain of irritable bowel syndrome, Proc. Natl. Acad. Sci. U.S.A. 115 (2018) E7438–E7447.
[10] A. Gidon, et al., Endosomal GPCR signaling turned off by negative feedback actions of PKA and v-ATPase, Nat. Chem. Biol. 10 (2014) 707–709.
[11] T.N. Feinstein, et al., Retromer terminates the generation of cAMP by internalized PTH receptors, Nat. Chem. Biol. 7 (2011) 278–284.
[12] N.B. Senese, M.M. Rasenick, J.R. Traynor, The role of G-proteins and G-protein regulating proteins in depressive disorders, Front. Pharmacol. 9 (2018) 1289.
[13] J.J. Tesmer, Structure and function of regulator of G protein signaling homology domains, Prog Mol Biol Transl Sci 86 (2009) 75–113.
[14] R.D. Teasdale, B.M. Collins, Insights into the PX (phox-homology) domain and SNX (sorting nexin) protein families: structures, functions and roles in disease, Biochem. J. 441 (2012) 39–59.
[15] B. Amatya, et al., SNX-PXA-RGS-PXC subfamily of SNXs in the regulation of receptor-mediated signaling and membrane trafficking, Int. J. Mol. Sci. 22 (2021).
[16] B. Zheng, et al., RGS-PX1, a GAP for GalphaS and sorting nexin in vesicular trafficking, Science 294 (2001) 1939–1942.
[17] C.M. Ha, et al., SNX14 is a bifunctional negative regulator for neuronal 5-HT6 receptor signaling, J. Cell Sci. 128 (2015) 1848–1861.
[18] Y. Zhang, et al., Structural studies reveal unique non-canonical regulators of G protein signaling homology (RH) domains in sorting nexins, J. Mol. Biol. 434 (2022) 167823.
[19] S. Pervaiz, Cell signaling and fate through the redox lens, Redox Biol. 25 (2019) 101298.
[20] H. Sies, C. Berndt, D.P. Jones, Oxidative stress, Annu. Rev. Biochem. 86 (2017) 715–748.
[21] C. Mas, et al., Structural basis for different phosphoinositide specificities of the PX domains of sorting nexins regulating G-protein signaling, J. Biol. Chem. 289 (2014) 28554–28568.
[22] L.S. Bernstein, A.A. Grillo, S.S. Loranger, M.E. Linder, RGS4 binds to membranes through an amphipathic α-helix, J. Biol. Chem. 275 (2000) 18520–18526.
[23] K. Su, et al., Structure of the PX domain of SNX25 reveals a novel phospholipid recognition model by dimerization in the PX domain, FEBS Lett. 591 (2017) 2011–2018.
[24] D.M. Berman, T.M. Wilkie, A.G. Gilman, GAIP and RGS4 are GTPase-activating proteins for the Gi subfamily of G protein alpha subunits, Cell 86 (1996) 445–452.
[25] D.E. Bosch, et al., A P-loop mutation in Galpha subunits prevents transition to the active state: implications for G-protein signaling in fungal pathogenesis, PLoS Pathog. 8 (2012) e1002553.
[26] J.J. Tesmer, D.M. Berman, A.G. Gilman, S.R. Sprang, Structure of RGS4 bound to AlF4–activated G(i alpha 1): stabilization of the transition state for GTP hydrolysis, Cell 89 (1997) 251–261.
[27] A.J. Kimple, et al., Structural determinants of G-protein alpha subunit selectivity by regulator of G-protein signaling 2 (RGS2), J. Biol. Chem. 284 (2009) 19402–19411.
[28] N.G. Tsvetanova, M. von Zastrow, Spatial encoding of cyclic AMP signaling specificity by GPCR endocytosis, Nat. Chem. Biol. 10 (2014) 1061–1065.
[29] D.D. Jensen, et al., Neurokinin 1 receptor signaling in endosomes mediates sustained nociception and is a viable therapeutic target for prolonged pain relief, Sci. Transl. Med. 9 (2017).
[30] I.H. Jang, et al., The direct interaction of phospholipase C-gamma 1 with phospholipase D2 is important for epidermal growth factor signaling, J. Biol. Chem. 278 (2003) 18184–18190.
[31] C.A. Elwell, et al., Chlamydia interfere with an interaction between the mannose-6-phosphate receptor and sorting nexins to counteract host restriction, Elife 6 (2017).
[32] B. Paul, et al., Structural basis for the hijacking of endosomal sorting nexin proteins by Chlamydia trachomatis, Elife 6 (2017).
[33] M.C. Zimmerman, A.J. Case, Redox biology in physiology and disease, Redox Biol. 27 (2019) 101267.
[34] A. Allegra, A. Tonacci, L. Giordano, C. Musolino, S. Gangemi, Targeting redox regulation as a therapeutic opportunity against acute leukemia: pro-oxidant strategy or antioxidant approach? Antioxidants 11 (2022).
[35] Y. Chen, J. Li, Z. Zhao, Redox control in acute lymphoblastic leukemia: from physiology to pathology and therapeutic opportunities, Cells 10 (2021).
[36] N. Mokrane, et al., Manipulations of glutathione metabolism modulate IP3-mediated store-operated Ca(2+) entry on astroglioma cell line, Front. Aging Neurosci. 13 (2021) 785727.
[37] W.-Z. Zhang, et al., The protein complex crystallography beamline (BL19U1) at the Shanghai Synchrotron Radiation Facility, Nucl. Sci. Tech. 30 (2019) 170.
[38] T.G.G. Battye, L. Kontogiannis, O. Johnson, H.R. Powell, A.G.W. Leslie, iMOSFLM: a new graphical interface for diffraction-image processing with MOSFLM, Acta Crystallogr. Sect. D Biol. Crystallogr. 67 (2011) 271–281.
[39] P.R. Evans, An introduction to data reduction: space-group determination, scaling and intensity statistics, Acta Crystallogr. Sect. D Biol. Crystallogr. 67 (2011) 282–292.
[40] A. Vagin, A. Teplyakov, MOLREP: an automated program for molecular replacement, J. Appl. Crystallogr. 30 (1997) 1022–1025.
[41] K. Cowtan, Fitting molecular fragments into electron density, Acta Crystallogr. Sect. D Biol. Crystallogr. 64 (2008) 83–89.
[42] G.N. Murshudov, et al., REFMAC5 for the refinement of macromolecular crystal structures, Acta Crystallogr D Biol Crystallogr 67 (2011) 355–367.
[43] Z.L. Chen, et al., A high-speed search engine pLink 2 with systematic evaluation for proteome-scale identification of cross-linked peptides, Nat. Commun. 10 (2019) 3404.
[44] L.H. Wang, et al., pFind 2.0: a software package for peptide and protein identification via tandem mass spectrometry, Rapid Commun. Mass Spectrom. 21 (2007) 2985–2991.